



universität
wien

DIPLOMARBEIT

Titel der Diplomarbeit

Synthesis of a 3-hydroxypyridin-4-one derivative for the
therapy of Parkinson's disease

and

Determining the penetration of hydroxypyridinones
through the Blood-Brain Barrier based on
co-culture systems

Verfasserin

Anna Preisner

angestrebter akademischer Grad

Magistra der Pharmazie (Mag. pharm.)

Wien, 2012

Studienkennzahl lt. Studienblatt:

A 449

Studienrichtung lt. Studienblatt:

Pharmazie

Betreuer:

O. Univ.-Prof. DI Mag. Dr. Christian Noe

Acknowledgements

First I would like to sincerely thank my Austrian supervisor Professor Christian Noe from the University of Vienna for giving me the chance to do this project at the King's College London. Moreover, I am grateful to Dr Hannelore Kopelent-Frank, the Erasmus coordinator of the University of Vienna for her support and time to answer all my questions regarding the Erasmus scholarship.

Furthermore, I would like to thank both of my supervisors in London, Professor Robert Hider from the *Chemical Biology* research group and Dr Jane Preston, who is part of the *Pharmacology and Therapeutics* research group. I am deeply grateful that Professor Hider and Dr Preston let me be a part of their working groups and for their support and encouragement throughout my stay in London. During these four months I was able to gain more knowledge about the blood-brain barrier and some *in vitro* experimental systems as well as about synthetic chemistry.

Likewise, I am truthfully grateful to PhD student Ana Georgian, of Dr Jane's group, who guided me through all the experiments concerning the blood-brain barrier and gave me an insight into this complex field. Moreover, I would like to thank PhD student Ferdinand Fuchs and Post-Doc Vincenzo Abbate for their help and advice on my synthetic work. I am grateful to Post-Doc Yongmin Ma and PhD Abdu Soltani, who introduced me into the work with the HPLC and took time to answer all my questions. I want to thank my colleagues, who worked with me in the lab for their support and for making my stay as pleasant as it was.

I want to particularly thank my parents and brother for their support and encouragement throughout the years of university and beyond.

Table of Contents

1	Introduction	8
1.1	Iron	8
1.1.1	Iron Chelators	8
1.1.2	Fields of application – Diseases of iron overload.....	10
1.1.3	Treatment of neurodegenerative diseases.....	11
1.1.4	Design of iron chelators	13
1.2	Blood-brain barrier.....	15
1.2.1	Function of the blood-brain barrier	15
1.2.2	History.....	15
1.2.3	Structure and cell types of the blood-brain barrier	16
1.2.4	Features of the BBB – Tight Junctions.....	17
1.2.5	Transports across the BBB	19
1.2.6	Blood-brain barrier in pathology	21
1.3	BBB – study approaches	21
1.3.1	In vivo	22
1.3.2	Ex vivo	22
1.3.3	In vitro	23
1.3.4	In silico.....	24
1.3.5	Transendothelial electric resistance – Indicator for BBB tightness.....	25
2	Aim of the project.....	26
3	Materials and methods.....	27
3.1	Materials.....	27
3.1.1	Instrumental details and equipment	27
3.2	Methods.....	29
3.2.1	Cell culture	29
1.1.1	Permeability assay.....	30

1.1.2	Sodium fluorescein – paracellular marker	31
3.2.2	Protein assay	32
3.2.3	HPLC system	32
3.2.4	Statistical analysis.....	32
4	Synthetic schemes	33
4.1	Synthesis of 2-methyl-3-benzyloxy pyran-4(1H)-one.....	33
4.2	Synthesis of 1-(2'-carboxyethyl)-2-methyl-3-(benzyloxy)-4(1H)-pyridinone.	34
4.3	Synthesis of 1-[2'-[(succinimidyloxy)carbonyl]ethyl)-2-methyl-3-benzyloxy)-4(1H)-pyridinone	35
4.4	Synthesis of 1,3,4,6-tetra-O-acetyl- β -D-glucosamine hydrochloride	36
4.5	Synthesis of N-(1,3,4,6-tetra-O-acetyl-2-deoxy- β -D-glucopyranos-2-yl)-3-(3-(benzyloxy)-2-methyl-4-oxopyridin-1(4H)-yl)propanamide	38
4.6	Deprotection of N-(1,3,4,6-tetra-O-acetyl-2-deoxy- β -D-glucopyranos-2-yl)-3-(3-(benzyloxy)-2-methyl-4-oxopyridin-1(4H)-yl)propanamide.....	39
5	Synthetic procedures.....	41
5.1	Synthesis of 2-methyl-3-benzyloxy pyran-4(1H)-one.....	41
5.2	Synthesis of 1-(2'-carboxyethyl)-2-methyl-3-(benzyloxy)-4(1H)-pyridinone.	42
5.3	Synthesis of 1-[2'-[(succinimidyloxy)carbonyl]ethyl)-2-methyl-3-benzyloxy)-4(1H)-pyridinone	44
5.4	Synthesis of 1,3,4,6-tetra-O-acetyl- β -D-glucosamine hydrochloride	47
5.5	Synthesis of N-(1,3,4,6-tetra-O-acetyl-2-deoxy- β -D-glucopyranos-2-yl)-3-(3-(benzyloxy)-2-methyl-4-oxopyridin-1(4H)-yl)propanamide	50
6	Results	53
6.1	HPLC of HPOs (CP20, YMF25, YMF24, YMF16)	53
6.2	Calibration curve – CP20.....	55
6.3	HPO BBB Permeability using non-contact co-culture PBEC model	56
6.4	HPO BBB Permeability using contact co-culture PBEC model.....	57
6.5	HPO BBB Permeability using non-contact co-culture PBEC model	59
7	Discussion	62

7.1	Changes in the analysis	63
8	Abstract.....	65
9	Zusammenfassung.....	67
10	Miscellaneous.....	69
10.1	References.....	69
10.2	Table of Formulas	72
10.3	Table of Figures	73
10.4	Table of Schemes	74
10.5	Table of Tables	75
10.6	List of Abbreviations.....	76
10.7	Curriculum vitae	78
Appendix	I
	NMR-selected data	II
	Mass spectrometry - spectrum.....	VII
	HPLC – AUCs of CP20 in water.....	VIII
	Picture of the research group.....	X
	To Whom It May Concern – by Professor R.C. Hider	XI

1 Introduction

1.1 Iron

Iron is an essential micronutrient for humans and other life forms (Oshiro, Morioka et al. 2011). Its ability to switch between the ferrous, Fe(II), and ferric, Fe(III) makes it indispensable as well as hazardous. Iron is a component of several enzymes and takes part in many vital biochemical activities, such as oxygen transport, energy metabolism and DNA-synthesis (Papanikolaou and Pantopoulos 2005).

The human body contains approximately 3-5g of iron, with more than two thirds found in hemoglobin, the protein of red blood cells. Around 20-30% of the body iron can be found in the liver and reticuloendothelial macrophages (Papanikolaou and Pantopoulos 2005; Oshiro, Morioka et al. 2011). The remaining body iron is localized in myoglobin, a protein that carries oxygen to muscles and in iron-containing proteins and enzymes (Papanikolaou and Pantopoulos 2005; Gkouvatsos, Papanikolaou et al. 2011) . The daily amount of absorbed iron from the diet is limited to 1-2 mg, which compensates for nonspecific iron losses (urine, stool, sweat) (Papanikolaou and Pantopoulos 2005; Supplements 2007).

Since there is no physiological pathway for iron excretion in humans, the maintenance of iron homeostasis and its regulation are necessary. Under physiological conditions extracellular iron is bound to plasma transferrin (Tf), in order to remain soluble and nontoxic (Papanikolaou and Pantopoulos 2005). Usually only one third of the circulating transferrin binds to iron, allowing the remaining Tf to buffer any alterations of iron levels. Under pathological iron overload Tf becomes fully saturated and unbound iron remains redox-active and thus toxic. An excess of iron induces the formation of radicals, which lead to cell death and tissue damage (Gkouvatsos, Papanikolaou et al. 2011).

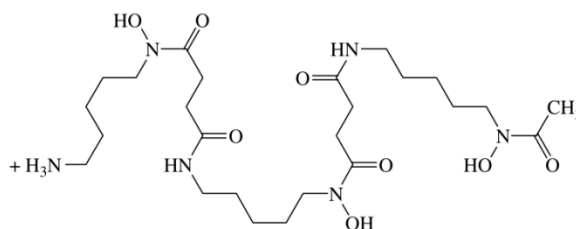
1.1.1 Iron Chelators

Iron chelators can reduce elevated levels of iron. Thus, organ damage caused by free iron can be prevented (Kwiatkowski 2008). The chelating agent could either form

a non-toxic complex with iron, which can be excreted or cover the metal at its protein binding site to suppress any redox activity (Gaeta, Molina-Holgado et al. 2011).

At this time, three iron chelators, Deferoxamine, Deferiprone and Deferasirox, are available for clinical use (Kwiatkowski 2008).

Deferoxamine (Formula 1) is produced in *Streptomyces pilosus* and has been used for over 40 years in patients with iron overload

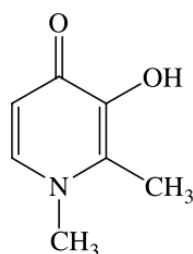


Formula 1 Deferoxamine

(Kwiatkowski 2008; Cappellini and Pattoneri 2009). It is a hexadentate iron

chelator, which binds iron in a 1:1 ratio. This complex is then excreted in urine and faeces. Unfortunately Deferoxamine is barely absorbed from the gastrointestinal tract and has a very short half-life. Therefore, it has to be administered subcutaneously or intravenously. The route and period of administration (over 8-24 hours, 5-7 days per week) led to the search for orally active iron chelators with a longer half-life (Kwiatkowski 2008).

Deferiprone (1,2-dimethyl-3-hydroxypyrid-4-one), the first orally active chelator

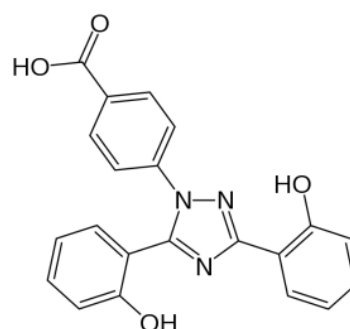


Formula 2
Deferiprone

was synthesized in the early 1980s (Formula 2). This chelating agent is hydrophilic and rapidly absorbed (Cappellini and Pattoneri 2009). Being a bidentate chelator it forms a 3:1 complex with iron, which is excreted in urine (Kwiatkowski 2008). Data from different studies showed that levels of other bivalent metals were not reduced significantly (Cappellini and Pattoneri 2009). Deferiprone has to be taken three times a day due to its short plasma half-life (1.5-2.5

hours). Unlike Deferoxamine, Deferiprone can cross cell-membranes and therefore protect organs, such as the heart and liver from iron overload (Cappellini and Pattoneri 2009). Adverse effects, such as neutropenia, and in rare cases agranulocytosis limit the use of deferiprone (Kwiatkowski 2008).

Deferasirox (Formula 3) is a novel, orally active iron chelator, which has to be taken only once a day (Kwiatkowski 2008). The active molecule is a highly



Formula 3 Deferasirox

lipophilic, N-substituted bis-hydroxyphenyl-triazole (Cappellini and Pattoneri 2009). The absorption from the gastrointestinal tract is rapid and the half-life, long (7-16h). Moreover Deferasirox has a high specificity for iron, with minimal affinity for other bivalent metals (Kwiatkowski 2008). It is able to remove iron from liver tissue. The tridentate chelator binds iron in a 2:1 ratio (Cappellini and Pattoneri 2009). Iron bound to Deferasirox is excreted in faeces (Kwiatkowski 2008). Reported adverse effects of Deferasirox include nephrotoxicity (Sanchez-Gonzalez, Lopez-Hernandez et al. 2011).

1.1.2 Fields of application – Diseases of iron overload

Hereditary hemochromatosis (HH) is the most common hereditary disease in populations of European ancestry (Sheftel 2001). It is an autosomal recessive disorder, which leads to an increased absorption of iron from the gastrointestinal tract. The excessive iron accumulates in different organs, causing severe damage. In most cases, HH results from a mutation of the HFE-gene, which plays an important role in the production of hepcidin (Papanikolaou and Pantopoulos 2005). Hepcidin, a liver-derived peptide hormone, is a regulator of iron homeostasis, preventing inappropriate high iron absorption. Circulating hepcidin is increased in the presence of iron and inflammation. In contrast, hepcidin levels are depressed in states of iron deficiency (Gkouvatsos, Papanikolaou et al. 2011). In patients with HH, hepcidin levels are low, despite of iron overload in several organs (Sheftel 2001). Accumulated iron is usually observed after the age of 40, mainly in the liver, but also the pancreas, heart and skin (Papanikolaou and Pantopoulos 2005).

A subtype of HH is juvenile hemochromatosis (JH), where a nonsense mutation in the hepcidin gene (HAMP) is responsible for the onset of the disease (Gkouvatsos, Papanikolaou et al. 2011). Patients suffering from JH will show symptoms before the age of 30 (Papanikolaou and Pantopoulos 2005).

Secondary iron overload develops in patients, who regularly receive blood transfusions (Sheftel 2001). Red blood cell transfusions are used for the treatment of chronic anemias, such as β -thalassemia major, sickle-cell disease, pyruvate kinase deficiency and other rare anemias (Kwiatkowski 2008). A unit of transfused blood contains 200-250mg of iron and patients with chronic anemias receive transfusions usually every 3-4 weeks (Kwiatkowski 2008; Cappellini and Pattoneri 2009). Moreover, in patients with ineffective erythropoiesis, iron absorption from the

gastrointestinal tract is highly increased (Kwiatkowski 2008). Regular administration of red cell transfusions and the inability of the human body to actively excrete iron lead to the accumulation of iron (Cappellini and Pattoneri 2009).

Iron overload is a critical state that harms the organism. Elevated levels of iron lead to cardiac toxicity, which is the leading cause of death in patients with iron-overload. Other affected organs are the liver and the endocrine system, resulting in complications, such as fibrosis, cirrhosis, growth failure and diabetes mellitus, respectively (Kwiatkowski 2008).

1.1.3 Treatment of neurodegenerative diseases

Elevated levels of redox active metals are found in the brain of patients with neurodegenerative diseases (ND), such as Alzheimer's disease, Parkinson's disease and Friedreich's ataxia (Hider, Roy et al. 2011). Chelation therapy is a reasonable approach to reduce the toxic levels of these metals, particularly iron. Therefore it is necessary to design chelating agents, which are able to cross to blood-brain-barrier and reach the brain (Hider, Ma et al. 2008).

Age is the main cause of most ND and this may be directly linked to oxidative stress. The definition of oxidative stress is described as an imbalance between the production and manifestation of free radicals and the organisms' ability to detoxify these reactive species through several enzymes, including superoxide dismutase, catalase and glutathione (Hider, Roy et al. 2011).

Reactive oxygen species (ROS) are small and highly unstable molecules, which contain oxygen. In order to become stable, free radicals are very likely to interact with molecules in the cell (lipids, protein, DNA), causing cytotoxicity. The most important free radicals are superoxide ($O_2^{\cdot-}$), peroxide (O_2^-) and hydroxyl radical (OH^{\cdot}). ROS are by-products of metabolic processes in the human body (Pantopoulos and Hentze 1995). Two major sources of ROS production are the mitochondrial respiratory chain and the cytochrome P450 mixed-function oxidases, a group of enzymes in the liver (Wu and Cederbaum 2003). Moreover, hydroxyl radicals can be generated by excessive free iron via the Fenton reaction ($Fe^{2+} + H_2O_2 \rightarrow Fe^{3+} + OH^{\cdot} + OH^-$). Thus elevated levels of unbound iron contribute to ROS production and oxidative stress (Molina-Holgado, Gaeta et al. 2008). Furthermore, free radicals from the environment, such as from radiation, smog, UV light or tobacco smoke, should not be neglected (Wu and Cederbaum 2003).

When the antioxidant capacity of the human body is reached, oxidatively modified molecules accumulate in cells, harming them and even leading to cell death (Hider, Roy et al. 2011). Compared with other organs, the brain is much more prone to oxidative damage due to its high consumption of oxygen and glucose, which leads to the production of reactive oxygen species. In addition, the levels of both iron and ascorbate are high, whereas levels of antioxidant protecting enzymes are low (Floyd and Hensley 2002).

In Europe around 10 million people have dementia, where the majority are diagnosed with AD and 1.2 million people suffer from PD (EPDA 2012; Parliament 2012). Both major neurodegenerative disorders, AD and PD, are associated with protein aggregation and oxidative stress (Gaeta, Molina-Holgado et al. 2011). In both of these metabolic alterations metal ions, such as iron and copper, are involved (Molina-Holgado, Gaeta et al. 2008). Moreover genetic factors play a role, as mutations in genes encoding aggregating proteins, such as amyloid beta protein and α -synuclein lead to inherited forms of AD and PD (Hider, Ma et al. 2008).

Alzheimer's disease (AD) is the most common form of dementia. It is a slowly progressing disease of the brain, which cannot be cured (Oshiro, Morioka et al. 2011). AD usually occurs after the age of 60. The risk of developing AD correlates with age and is between 10-15% at the age of 65. The risk rises even up to 50% for those over the age of 85. Moreover, there is also a form with an early onset. In this case, genetic factors play a major role and symptoms can occur at the age of 30-40. Nevertheless, both forms have similar symptoms, including mild cognitive impairment and loss of memory in early stages. Later on, affected people lose the ability to cope with everyday functions, such as dressing, standing, walking, and even swallowing. In addition, the behaviour changes and patients can become depressed or withdrawn, or on the other hand, depressive or hostile (Burd, Fraser et al. 2001). The AD brain is characterized by insoluble aggregates of amyloid beta protein between nerve cells and neurofibrillary tangles inside the neurons (Burd, Fraser et al. 2001; Oshiro, Morioka et al. 2011). Furthermore, the levels of the neurotransmitter acetylcholine are low in brain regions, which are responsible for short-term memory, memory storage and behaviour (Burd, Fraser et al. 2001).

Parkinson's disease is a slowly developing neurodegenerative disorder, affecting the movement, with no cure. There are also two forms, comparable to AD, the familial and the sporadic form. The familial form is caused by genetic mutations

with an early onset, around the age of 40. The causes of the sporadic form are for the most part unknown. Risk factors such as, age, gender (men are more often affected than women) and environmental influences play a role. The average age of outbreak is around 60 years (Burd, Fraser et al. 2001). Parkinson's disease (PD) is caused by the death of dopamine-generating cells in the substantia nigra (SN) and elevated levels of acetylcholine in the striatum (Oshiro, Morioka et al. 2011). Dopamine is a neurotransmitter, which is necessary for normal muscle activity. Therefore the cardinal symptoms of PD result from altered muscle function (Burd, Fraser et al. 2001). Moreover, Lewis bodies, intracytoplasmic inclusions in the SN, are considered as the hallmark of PD and consist mostly of phosphorylated α -synuclein (Oshiro, Morioka et al. 2011).

Patients suffer from tremors in the hands and feet, rigidity, bradykinesia due to excessive muscle contraction caused by decreased dopamine levels (Burd, Fraser et al. 2001; Oshiro, Morioka et al. 2011). Non-motor symptoms include cognitive impairment, mood swings and sleep disturbances. Many affected people also suffer from depression (Oshiro, Morioka et al. 2011).

1.1.4 Design of iron chelators

Iron chelators for clinical use must fulfil many criteria, with metal selectivity being of utmost importance. Moreover membrane permeability is important in order to reach the target tissue and oral activity is advantageous. Factors like lipophilicity, molecular size and ionization state affect the permeability of membranes and need to be considered (Liu and Hider 2002). First of all the target metal has to be identified. Pathogenesis and progression of neurodegenerative diseases are complex and many factors are involved. However, iron could be assigned as the main target in PD. In contrast, in AD also copper and zinc play a crucial role in the progression of the disease and designing a chelator suitable for these metals is intricate and the toxic potential will be high (Gaeta and Hider 2005).

In the design of iron chelators the oxidative state of the target metal is important and affects the choice of the donor atoms. Iron(II) selective chelating agents possess nitrogen or sulfur atoms as ligands, whereas chelators with high affinity for iron(III) contain oxygen atoms as ligands (Gaeta and Hider 2005). Iron(II) selective chelators will bind other essential bivalent metals, such as zinc, copper and cobalt to a certain degree, which can result in toxicity. In contrast, most tribasic

cations, including aluminium and gallium, are not essential to living cells, because they have no vital functions. This renders iron(III) as the preferred oxidative state for iron chelation (Liu and Hider 2002).

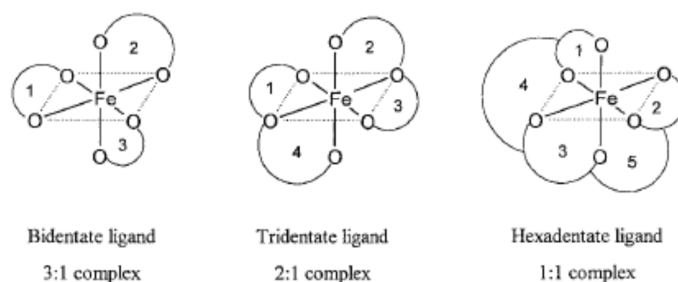


Figure 1 Schematic representation of chelate ring formation in metal-ligand complexes (taken from Liu and Hider (2002)).

Chelating agents, not only possess different donor atoms, moreover the number of the ligands can vary. Chelators with two, three, six or more ligands can be classified as bi-, tri-, hexa- or multidentate chelators, as shown in Fig. 1 (Gaeta and Hider 2005). Regarding BBB permeability and oral absorption the size of the chelating agents should be < 300 kDa, thereby excluding hexadentate chelators. Moreover molecules should be uncharged and possess appreciable lipid solubility ($\log P > -0.7$) in order to penetrate membranes (Liu and Hider 2002).

Generation of non-toxic chelating agents is crucial for clinical use. Toxicity can result from many factors, which need to be considered, such as inhibition of iron-containing metalloenzymes, lack of metal selectivity and redox cycling of iron complexes between the iron(II) and iron(III), which generates free hydroxyl radicals. Moreover kinetic liability of iron complexes can lead to redistribution of iron causing cell injury and death (Gaeta and Hider 2005).

The group of bidentate hydroxypyridin-4ones are suitable for therapy of PD, because they possess high affinity for iron(III) and form neutral 3:1 complexes under physiological conditions. The main problem is the kinetic liability which in principle can lead to the generation of free hydroxyl radicals. Different substitutions at the pyridinone ring can affect the properties of the chelating agents and lead to effective compounds, with low toxicity (Liu and Hider 2002).

1.2 Blood-brain barrier

1.2.1 Function of the blood-brain barrier

The blood-brain barrier (BBB) is formed by endothelial cells of the brain capillaries (Abbott, Patabendige et al. 2010). It is a selective interface between the blood and the central nervous system (CNS) with vital functions, such as protection against toxic and noxious compounds. An essential function of the BBB is the maintenance of the brain homeostasis by controlling the concentration of ions within the brain (Cardoso, Brites et al. 2010). In order to generate optimal conditions for synaptic signalling, exchanges between the blood and brain compartments are regulated by specific ion channels and transporters (Abbott, Patabendige et al. 2010). Some neurotransmitters achieve high levels in the blood plasma, especially after meals or exercise, which could be detrimental to the brain tissue if allowed to freely diffuse into the brain. Therefore, the BBB has to separate between two pools of neurotransmitters, central and peripheral. On that account, the central and peripheral nervous system can use similar or the same agents in different concentrations without affecting the other (Abbott, Ronnback et al. 2006; Bernacki, Dobrowolska et al. 2008).

Being a selective barrier, the BBB has to differentiate between nutrients and metabolites required by the CNS and toxic or noxious substances. Therefore, the BBB possesses a number of efflux transporters to remove unwanted agents, such as xenobiotics, some endogenous metabolites and microorganisms (Abbott, Patabendige et al. 2010). Essential nutrients can enter the brain through passive permeability or specific transport systems in order to keep a constant supply of the required substrates (Abbott, Patabendige et al. 2010; Cardoso, Brites et al. 2010).

The BBB is present in all brain regions, except those, which regulate the autonomic nervous system and endocrine glands of the body. In these areas, blood-borne molecules can diffuse through fenestrations in blood vessels (Ballabh, Braun et al. 2004).

1.2.2 History

In 1885, Paul Ehrlich, a German scientist and physician, experimented with vital dye and its impact on mammals. The dye was injected intravenously into rats and stained all the organs of the body except the brain and spinal cord. He assumed

that the brain had less affinity to the dye than the other parts of the body (Ehrlich 1885). One of Ehrlich's students, Edwin Goldmann continued Ehrlich's work. He injected trypan blue intravenously observing the same result as Ehrlich. Moreover he performed additional experiments where the dye was injected directly into the cerebrospinal fluid. This time the CNS was dyed and the other organs remained unstained. Goldmann presumed that a barrier must exist between the blood and the central nervous system. Max Lewandowsky, a German neurologist, studied the low permeability of potassium ferrocyanate into the brain and was the first to use the term "blood-brain barrier" (Cardoso, Brites et al. 2010).

1.2.3 Structure and cell types of the blood-brain barrier

The BBB is mainly formed by three different cell types: endothelial cells of the capillaries, astrocyte's endfeet, which form a fine lamellae around the capillary endothelium and pericytes, which cover up to 30% of the capillaries. Moreover, the basement membrane, neurons and neighbouring microglia cells are crucial for the proper function of the CNS. Due to their interactions and functions all these cell types are constituent parts of the neurovascular unit (NVU) (Fig. 2) (Cardoso, Brites et al. 2010).

Endothelial cells (ECs) are essential for the BBB properties, as experiments showed that the endothelial layer could not be crossed by horseradish peroxidase from either side. Furthermore, experiments with amphibian's brains showed a high electrical resistance, indicating that they are impermeable to ions. The neurovascular unit of amphibians does not possess astrocytes, which proved the importance of the ECs for the BBB features (Hawkins, O'Kane et al. 2006).

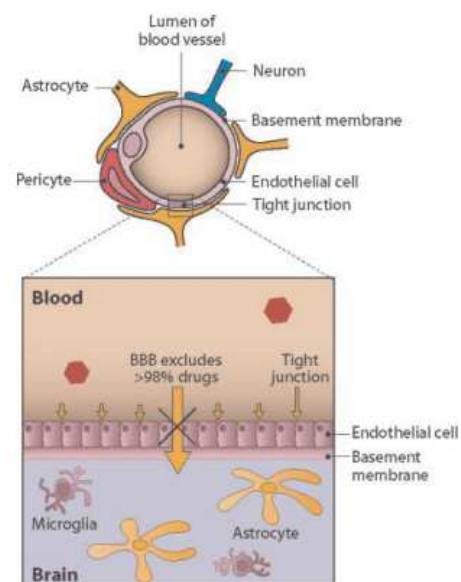


Figure 2 Schematic representation of the NVU (taken from Mensch, Oyarzabal et al. (2009).

Astrocytes, whose endfeet envelop the capillary endothelium, are necessary for proper neuronal function. Moreover astrocytes are able to enhance the charge selectivity of ECs by increasing the production of proteoglycan, which forms the

negatively charged glycocalyx (Abbott, Patabendige et al. 2010; Cardoso, Brites et al. 2010). Despite being an important part of the NVU, in some part of the CNS the endothelia lack astrocyte envelopment (Abbott 2002). Cell culture experiments, where cells were grown in non-contact co-culture using an astrocytes-conditioned medium, showed the secretion of factors by the astrocytes. The presence of these factors leads to a rise of tight junctional proteins and limits the transport across the BBB (Cardoso, Brites et al. 2010). The close association between ECs and astrocytes is crucial for the function and properties of the BBB (Abbott, Patabendige et al. 2010).

Pericytes, vascular smooth muscle cells, cover up to 30% of the endothelia and play an important role in the proliferation and differentiation of ECs (Kim, Tran et al. 2006; Dore-Duffy 2008). In addition to structural support, pericytes can also modulate the permeability of the BBB (Cardoso, Brites et al. 2010). In critical situations, such as hypoxia, pericytes migrate away from the microvessels and increase the transport across the BBB (Hawkins and Davis 2005).

1.2.4 Features of the BBB – Tight Junctions

A key feature of the BBB are tight junctions, which keep macromolecules and polar solutes from the entering the brain through paracellular diffusion (Abbott, Patabendige et al. 2010). Junctional complexes form a solid barrier by connecting ECs tightly together, eliminating gaps and spaces between the cells (Cardoso, Brites et al. 2010). Tight junctions and adherens junctions ensure that only a limited number of molecules, such as O₂ and CO₂ can pass the BBB freely. Gap junctions between ECs have been identified as a part of the BBB, but their impact on the barrier has yet to be discovered (Abbott 2002; Cardoso, Brites et al. 2010).

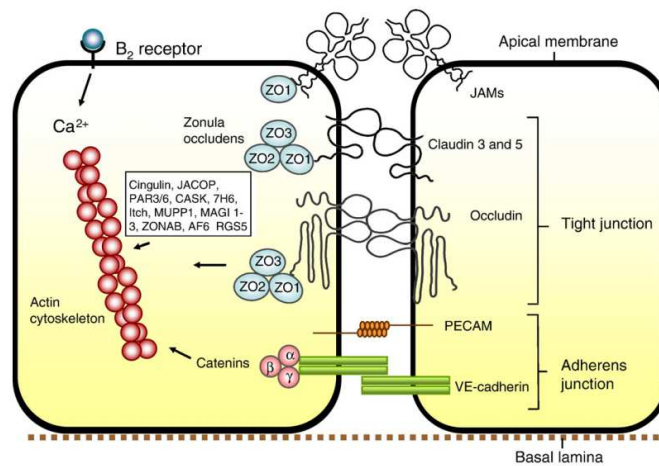


Figure 3 Structure of the BBB tight junctions (taken from Abbott, Patabendige et al. (2010). Further explanation in the text.

Tight junctions (Fig. 3) are located in the apical area of the ECs and influence the properties of the BBB greatly (Cardoso, Brites et al. 2010). The complex structure of TJ is formed by various proteins, such as transmembrane proteins occludin and claudin (Abbott, Patabendige et al. 2010). These proteins interact with proteins, which are located in the plasma membrane of the neighbouring cell, such as ZO-1, ZO-2 and ZO-3 (Petty and Lo 2002). Depending on how many times the transmembrane proteins span the plasma membrane, they are divided into groups. Occludin and claudin have four-pass transmembrane domains and are crucial for the tightness of the BBB in contrast to single-pass proteins, junctional adhesion molecules (JAM) (Cardoso, Brites et al. 2010).

To date, 24 isoforms of claudin are known, with approximately 20-27 kDa (Persidsky, Ramirez et al. 2006; Zlokovic 2008). Despite of sharing the four transmembrane domains with occludin, both proteins consist of completely different amino acids (Cardoso, Brites et al. 2010). Some claudins are essential for the maintenance of proper BBB function and experimental data showed that lack of claudin-3 or claudin-5 results in a highly permeable BBB (Abbott, Patabendige et al. 2010).

Occludin, a transmembrane protein of approximately 65 kDa modulates the permeability of the BBB to ensure that large, charged and polar molecules cannot cross the BBB readily (Furuse, Hirase et al. 1993; Huber, Egleton et al. 2001). Moreover occludin takes part in the differentiation of ECs and signal pathways (Cardoso, Brites et al. 2010). Nevertheless, experiments with knockout mice showing that a lack of occludin can be compensated by other junctional proteins and the

functions and properties of the BBB are retained (Hawkins, O'Kane et al. 2006; Zlokovic 2008).

Adherens junctions, located below the TJ, are of great importance for the formation of TJ by providing structural support and holding cells together (Abbott, Patabendige et al. 2010; Cardoso, Brites et al. 2010). Cadherin, a Ca^{2+} dependent transmembrane protein is linked to a protein of the catenin family (Cardoso, Brites et al. 2010). To date four catenins, alpha, beta, delta and gamma are known. Their main purpose is the connection of the cadherin complex to the actin filaments on the surface of ECs, forming a bridge between two cells (Cardoso, Brites et al. 2010).

Junctional complexes have a dynamic structure and react to changes in conditions during health and pathology. Under certain conditions, junctional proteins can disintegrate and reassemble in order to modulate the permeability of the BBB. Several kinases, such as mitogen-activated protein kinases, are involved in this process (Cardoso, Brites et al. 2010). The connection between protein phosphorylation and changes in the structure of TJ was confirmed by observations of the scaffolding protein ZO-1. The degree of phosphorylated ZO-1 was much higher in low resistance cells than in those with a high resistance to ion movement (Stevenson, Anderson et al. 1989). Furthermore, second messenger Ca^{2+} can also modulate the tightness of the BBB. Transmembrane protein cadherin is Ca^{2+} -dependent and the structure of AJs is broken at low concentrations of Ca^{2+} , leading to hyperpermeability of the BBB (Cardoso, Brites et al. 2010).

1.2.5 Transports across the BBB

The properties and functions of the BBB hinder a number of compounds and essential nutrients from entering the CNS freely (Cardoso, Brites et al. 2010). Moreover, a number of different factors keep molecules from entering the CNS, such as a high polar surface and a molecule weight above 450 kDa. In addition, molecules with more than 6 hydrogen acceptors are limited in the passive transport across the BBB, because their movement into the lipid of the cell membrane requires a lot of energy. Therefore many different transport mechanisms, depending on properties and size of the compounds, exist to transfer these molecules across the BBB, as shown in Fig. 4 (Abbott, Patabendige et al. 2010). Small molecules can use the paracellular pathway to cross the BBB, charged and polar molecules have to be transported via the transcellular pathway (Petty and Lo 2002).

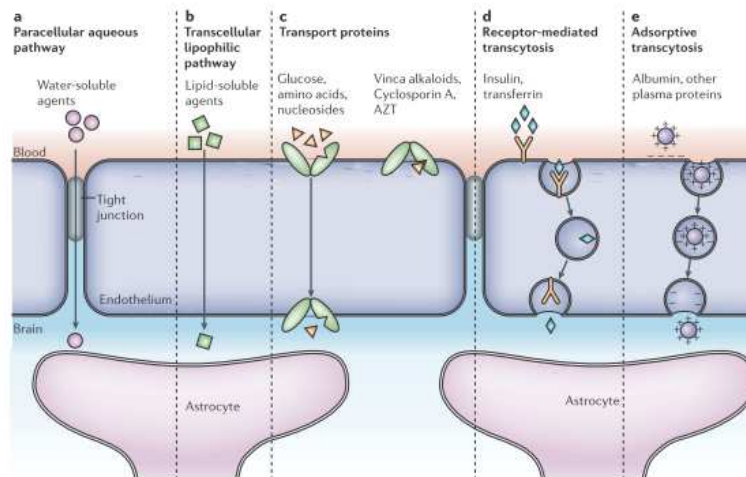


Figure 4 Pathways across the BBB (taken from Abbott, Ronnback et al. (2006). Further explanation in the text.

Small, lipid-soluble and unipolar molecules, including ethanol, cross the BBB by passive diffusion. Blood gases, oxygen and carbon dioxide, move down their concentration gradients by diffusion, blood-flow dependent. The supply of gases is sufficient as long as physiological blood-flow is warranted (Abbott, Patabendige et al. 2010).

Solute carriers, located in ECs of the BBB, facilitate the transport of polar compounds, such as glucose or amino acids to the CNS. Furthermore, small peptides, free fatty acids, organic anions and cations are transported by solute carriers (Abbott, Patabendige et al. 2010). Depending on the direction of the transport – from blood to brain or from brain to blood – solute carriers are inserted into either luminal, abluminal or both membranes of ECs (Abbott 2002; Bernacki, Dobrowolska et al. 2008). Glucose transporter-1 (GLUT-1) ensures sufficient supply of glucose, the main energy source of the CNS (Persidsky, Ramirez et al. 2006). This solute carrier is inserted into both ECs membranes, with more GLUT-1 molecules in the abluminal membrane. This uneven distribution prevents the risk of glucose-accumulation at levels higher than those in the blood (Cardoso, Brites et al. 2010).

Beside supplying the CNS with essential nutrients through soluble carriers, specific transporters in the BBB protect the brain from toxic and noxious substances by pumping them out of the brain compartment (Abbott, Patabendige et al. 2010). ATP-binding cassette transporters (ABC-transporters) are a superfamily of proteins with 48 members, divided into 7 sub-families (Dean, Rzhetsky et al. 2001). The most studied ABC-transporters for humans are P-glycoprotein (Pgp, Multidrug Resistance Protein, ABCB1), the Multidrug Resistance-associated Proteins (MRPs, ABCC1, 2, 4 and 5) and Breast Cancer Resistance Protein (BRCP, ABCG2). In order to efflux

compounds actively out of the CNS, ABC-transporters are ATP-dependent (Abbott, Patabendige et al. 2010). The substrates for ABC-transporters are lipid-soluble compounds, such as neurotoxic molecules, whose removal protects the functions of the brain. Moreover, many drugs can be actively effluxed out of the brain, so increasing the lipid solubility of a drug does not guarantee penetration into the brain (Dauchy, Dutheil et al. 2008; Abbott, Patabendige et al. 2010).

Macromolecules, such as proteins or peptides cross the BBB via endocytotic mechanisms. The transcytosis can be receptor-mediated (RMT) or absorptive-mediated (AMT). In RMT ligands (e.g. Fe-transferrin) have to bind specific receptors (Transferrin) on the surface of ECs and a caveolus is formed. This vesicle crosses the cytoplasm of the endothelia and the internalised ligand is released at the other side (Abbott, Patabendige et al. 2010). In the AMT mechanism the protein has to be in the cationic form (cationised albumin) to merge with the binding sites on the surface and start the endocytosis followed by transcytosis and finally exocytosis (Sauer, Dunay et al. 2005). Both mechanisms ensure that macromolecules can cross the BBB intact (Abbott, Patabendige et al. 2010).

1.2.6 Blood-brain barrier in pathology

Dysfunctions of the BBB are a part of several CNS pathologies, such as Parkinson's disease, Alzheimer's disease, epilepsy, multiple sclerosis, glaucoma and brain tumours (Abbott, Patabendige et al. 2010). The degree of the dysfunction differs and can even lead to total breakdown of the protective barrier function (Forster 2008). When transport mechanisms become ineffective, toxic or noxious compounds can reach the brain, accumulating and causing damage. Moreover the supply of the brain with essential nutrients may become insufficient. Changes of BBB functions and compositions accelerate the progress of the CNS diseases, although it is unknown whether BBB dysfunctions play a role in the onset of the diseases (Abbott, Patabendige et al. 2010).

1.3 BBB – study approaches

The increasing number of neurodegenerative diseases, including PD and AD along with the pathological changes of the CNS led to a high interest in the BBB (Mensch, Oyarzabal et al. 2009). Moreover the BBB prevents > 98% of drugs from

entering the brain and BBB models are used to investigate properties of the BBB as well as transport mechanisms and test the ability of compounds to cross the BBB (Tosi, Costantino et al. 2008). There are different approaches to study the BBB – *in vivo*, *ex vivo*, *in vitro* and *in silico* – with every system having its advantages and disadvantages (Cardoso, Brites et al. 2010).

1.3.1 In vivo

The *in vivo* system provides the most reliable reference information for testing and validating other models (Pardridge 1999). This experimental system allows analysis of the whole brain and its biological processes (Cardoso, Brites et al. 2010). *In vivo* methods can be classified into invasive and non-invasive techniques and are used to investigate brain metabolism, transport mechanisms, neurological disease progression, drug biodistribution and BBB disruption (Mensch, Oyarzabal et al. 2009; Cardoso, Brites et al. 2010). *In vivo* experiments are mainly performed on brains of murines and primates using techniques, such as *in vivo* intravenous administration and *in situ* brain perfusion (Mensch, Oyarzabal et al. 2009; Cardoso, Brites et al. 2010). Different knockout animals for BBB proteins have been used to determine permeability properties and study TJ functions (Furuse 2009). However, it needs to be taken into account that results from animal brains cannot be directly translated to humans (Cardoso, Brites et al. 2010). Moreover, experiments on living animals require expensive equipment and a large number of animals (Cohen-Kashi Malina, Cooper et al. 2009; Cardoso, Brites et al. 2010).

1.3.2 Ex vivo

Ex vivo studies are performed on living tissue in a highly controlled environment (Cardoso, Brites et al. 2010). Tissue from brain specific regions is easily obtained and in contrast to *in vivo* models, more invasive studies can be performed, such as immunocytochemical procedures or fluorescent nuclear staining (Lossi, Alasia et al. 2009; Cardoso, Brites et al. 2010). Investigation of whole organs or systems is possible with *ex vivo* experimental systems providing information on neurological diseases, infectious diseases, neurovascular homeostasis and hypoxia. Furthermore, post-mortem tissue can be used to study TJ, basement membrane assembly along the evaluation of brain capillary permeability and expression of efflux

proteins. Limitations of the *ex vivo* models include the artificial environment and the rarity of human living samples. Moreover *ex vivo* experiments allow only short-term experiences (Cardoso, Brites et al. 2010).

1.3.3 In vitro

The *in vitro* experimental system is a simplified model of the *in vivo* one (Cecchelli, Berezowski et al. 2007). *In vitro* models should be reproducible and mimic as closely as possible the *in vivo* barrier (Gumbleton and Audus 2001). *In vitro* models consist mainly of EC, since they are considered to be the anatomic basis of the BBB (Cardoso, Brites et al. 2010). To date several *in vitro* models are available to study BBB permeability and properties despite being difficult to reproduce and are time-consuming (Abbott 2002; Aschner, Fitsanakis et al. 2006). Many species are used for *in vitro* studies, including brain tissue from rodents, porcine and bovine (Cardoso, Brites et al. 2010).

The easiest way to mimic the BBB are cell lines, which are generated by immortalization of brain capillary endothelial cells (BCEC) using different immortalizing genes. Cell lines grow faster than primary cells and allow a large number of experiments in short time (Gumbleton and Audus 2001). Fields of study include transport systems, inflammatory cascades and toxicity modulation (Cardoso, Brites et al. 2010). However, cell lines cannot be used for permeability experiments since they only possess leaky intercellular junctions and lack paracellular junctions (Gumbleton and Audus 2001).

Primary cultures of BCEC present a more challenging *in vitro* model to investigate the BBB (Smith, Omid et al. 2007). The monolayer of BCEC is grown on a microporous membrane filter culture insert, as shown in Fig.5A (Cohen-Kashi Malina, Cooper et al. 2009). Due to the limited availability of human brain tissue, bovine and porcine tissues are mainly used (Cecchelli, Berezowski et al. 2007). It is difficult to obtain pure EC, since all components of the NVU are very close together and it is intricate to remove all cells that envelop the EC. Moreover this model does not take the microenvironment into account (Calabria, Weidenfeller et al. 2006). Primary cultures are used for studies of neuroinflammation and disease processes as well as CNS drug delivery (Cardoso, Brites et al. 2010).

A more complex *in vitro* model are co-cultures, which take the importance of astrocytes into account (Cecchelli, Berezowski et al. 2007). Experiments showed that

astrocytes play a crucial role in the development of TJ. Moreover, co-cultures make it possible to investigate interactions between EC and other components of the NVU (Abbott, Ronnback et al. 2006). BCEC are co-cultured mainly with glial cells from rat brain and can be used to study BBB permeability (Cardoso, Brites et al. 2010). Due to the similar vascular physiology of the porcine and the human brain, porcine co-culture models are suitable for studying the BBB. The co-culture experimental system can be either a non-contact co-culture with the glial cells seeded at the bottom of the Transwell (Fig. 5B) or a contact co-culture where the porcine brain endothelial cells (PBEC) are grown on the upper side of the Transwell membrane and the glial cells seeded on the underside of the filter membrane (Fig.5C). Contact co-culture models achieved the highest TEER measurements and display the closest anatomical features to the *in vivo* situation (Cohen-Kashi Malina, Cooper et al. 2009).

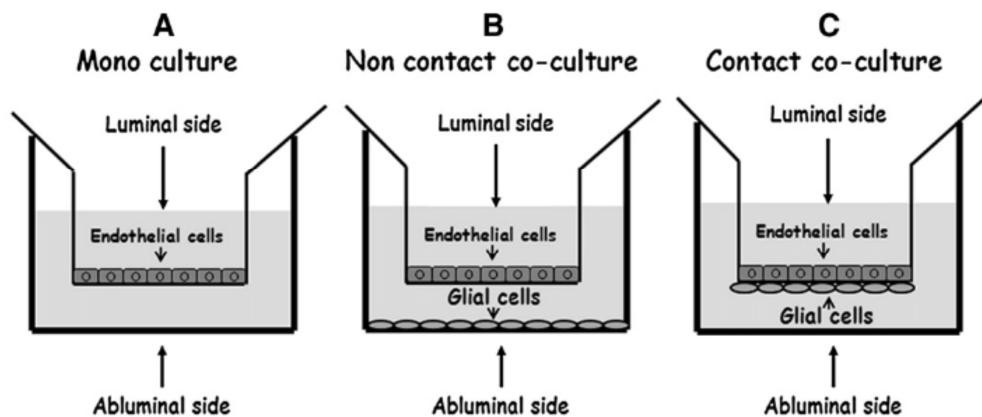


Figure 5 Schematic drawings of three *in vitro* BBB culture systems (taken from Cohen-Kashi Malina, Cooper et al. (2009)).

1.3.4 *In silico*

In silico prediction methods are cheaper and less time-consuming than the *in vivo* and *in vitro* experimental systems, because large numbers of compounds can be screened rapidly (Mensch, Oyarzabal et al. 2009). Experimental data from *in vivo* methods provides the base for the computational models and algorithms (Cardoso, Brites et al. 2010). *In silico* methods are used to predict the ability of drugs to enter the brain (Mensch, Oyarzabal et al. 2009). Computer programmes, such as *pCEL-X* or *pION* can be used to model the various factors controlling transport of drug-like molecules across membranes in permeability measurements (Avdeef and Tsinman). Moreover transporters properties and protein activity can be predicted as well as toxicity evaluation (Cardoso, Brites et al. 2010). It has to be considered that *in silico*

methods are based on prediction models, use only total concentrations for modelling and cannot include the whole complexity and interactions of the BBB (Cardoso, Brites et al. 2010).

1.3.5 Transendothelial electric resistance – Indicator for BBB tightness

There are many indicators of BBB properties. Transendothelial electric resistance (TEER) has been considered to be the most accurate measurement of BBB tightness and barrier function (Cardoso, Brites et al. 2010). It is a useful indicator of paracellular ion flux as it reflects the impedance to the passage of small ions through a physiological barrier (Cohen-Kashi Malina, Cooper et al. 2009). There are plenty

methods to measure TEER, which is expressed in $\Omega \cdot \text{cm}^2$. The simplest method requires a voltohmmeter coupled to a pair of electrodes (Fig.6), which is accessible to most laboratories. Other systems (e.g. Electrical Cell-substrate Impedance Sensing (ECIS)) require more sophisticated equipment, which is connected to a computer for continuous measurement of TEER (Cardoso, Brites et al. 2010). A high

quality in vitro model should attain high TEER measurement. Overall, average TEER values of monocultures are around $100 \Omega \cdot \text{cm}^2$. Using contact co-culture TEER values can be increased up to $1650 \Omega \cdot \text{cm}^2$ (Cohen-Kashi Malina, Cooper et al. 2009).

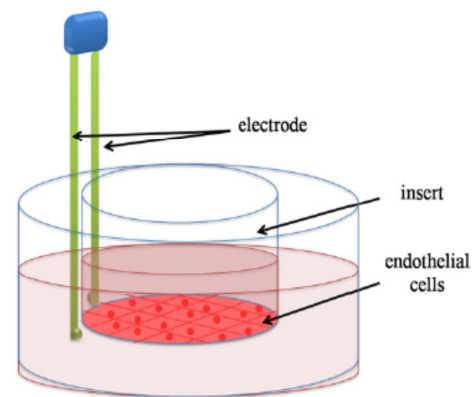
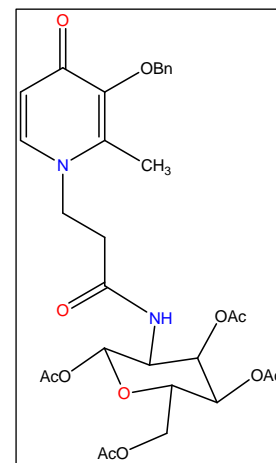


Figure 6 Schematic representation of the transendothelial electrical resistance measurement with electrodes (taken from Cardoso, Brites et al. (2010)).

2 Aim of the project

The aim of my four month project at King's College London (KCL) was to gain more knowledge in organic chemistry and the synthesis of iron chelators aimed towards the treatment of Parkinson disease.

One objective was to synthesis an iron chelator, which is coupled with a sugar molecule (Formula 4), since a sugar should enhance the chelators ability to enter the brain, which is the major target area for chelator therapies in Parkinson disease. Ideally, it was also aimed to assess whether the iron chelator was capable of entering the brain by determining whether it could cross the blood-brain barrier (BBB), which is a both a physical and metabolic barrier that exists between the blood and brain parenchyma that is known to restrict drug entry to the brain .



Formula 4 Structure of the desired iron chelator

The synthesis and biological studies of the iron chelators are part of a collaborating project between the *Pharmacology and Therapeutics* and *Chemical Biology* research groups of the KCL. Professor Robert C. Hider and his PhD student Ferdinand C. Fuchs were advising and helping me during the synthetic process of my project. Moreover I got an insight on the wide field of the BBB and *in vitro* experimental systems, during my work in the research group of Dr Jane Preston.

In order to test the synthesized iron chelator for its ability to cross the BBB, two different co-culture experimental systems were investigated for suitability. Four hydroxypyridin-4-one (HPO) derivatives with known properties were used to compare a contact co-culture with a non-contact co-culture experimental system, under the guidance of PhD student Ana Georgian.

3 Materials and methods

3.1 Materials

3.1.1 Instrumental details and equipment

3.1.1.1 Nuclear magnetic resonance

Nuclear magnetic resonance (NMR) spectra were recorded using a Bruker 400 (400 MHz) NMR spectrometer. Chemical shifts (δ) are reported in ppm downfield from the internal standard tetramethylsilane (Me_4Si , $\delta=0$). The notations s (singlet), d (doublet), t (triplet), q (quartet) and m (multiplet) were used to describe the resonance patterns. NMR samples were prepared by dissolving ~10mg of the compound in 0.5 mL deuterated solvent. Data from the spectrometer was analysed using the software MestReNova (Mnova).

3.1.1.2 Melting points

An Electrothermal IA 9100 Melting Point Apparatus was used to determine the melting points.

3.1.1.3 Chromatography

Aluminum plates coated with silica gel 60 F₂₅₄ from Merck were used for thin layer chromatography. When column chromatography was applied, silica gel 40-63 μm , technical grade from Sigma-Aldrich was used.

3.1.1.4 Mass spectrometry

A ThermoFinnigan LCQ Deca XP (electro-spray ionization, ESI) spectrometer was used for mass spectrometry. The procedure was carried out by the Centre of Excellence for Mass Spectrometry (CEMS-Waterloo) at the Waterloo campus of the King's College London. The sample was prepared by dissolving 1 mg of the compound in 1 mL of MeOH.

3.1.1.5 High pressure liquid chromatography

High pressure liquid chromatography (HPLC) was conducted on a Waters system with a 717plus Autosampler, a 2996 Photodiode Array Detector, a 600s Controller and a 626 pump was used for HPLC, all purchased from Waters. The column used

was a reversed phase polymer column, PLRP-S, 300 Å, 8µm, 15 cm obtained from Waters.

3.1.1.6 Chemicals

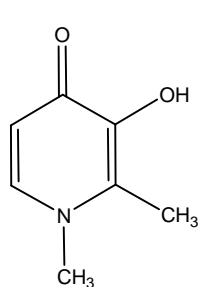
All reagents and solvents were purchased from Sigma-Aldrich, Alfa-Aesar, Fisher Scientific, Fluka and Acros Organics, unless stated otherwise. The chemicals were in reagent or analytical grade and used without further purification.

3.1.1.7 Cells

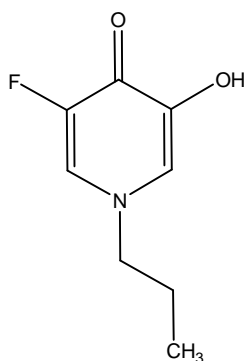
The cells used to perform the experiments were provided by PhD student Ana Georgian from King's College London.

3.1.1.8 Hydroxypyridinones (HPOs)

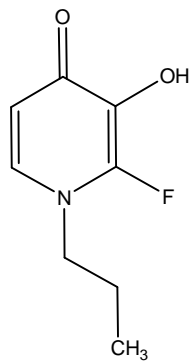
CP20 (deferipron), YMF-25, YMF-24 and YMF-16 (Formula 5) were used in this study. Deferipron was used as a control, because of its known ability to cross the BBB and was purchased from Sigma-Aldrich. The others HPOs, YMF-25, YMF-24 and YMF-16 were already tested for their ability to cross the BBB in an *in vivo* system. In order to compare the *in vivo* and *in vitro* model the same HPOs were used. YMF-25, YMF-24 and YMF-16 were provided by Post-Doc Yongmin Ma from King's College London.



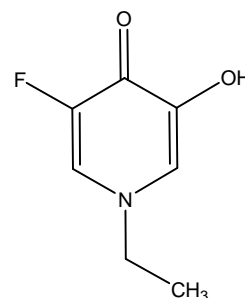
CP20=Deferiprone
MW 139.15



YMF 25
MW 171.17



YMF 24
MW 252.08



YMF 16
MW 157.17

Formula 5 Structures of the tested HPO-derivatives

3.2 Methods

3.2.1 Cell culture

The porcine brain endothelial cells (PBECS) were grown in co-culture with rat C6 glioblastoma cells in 12-well 0.4µm pore, polycarbonate Transwells (Costar) (Figure 7). In order to evaluate two systems, the cells were grown in non-contact co-culture as well as in contact co-culture; with PBECS grown on the top-side of the transwell, with C6 cells either on the bottom of the chamber below or on the underside of the Transwell-filter itself, respectively.

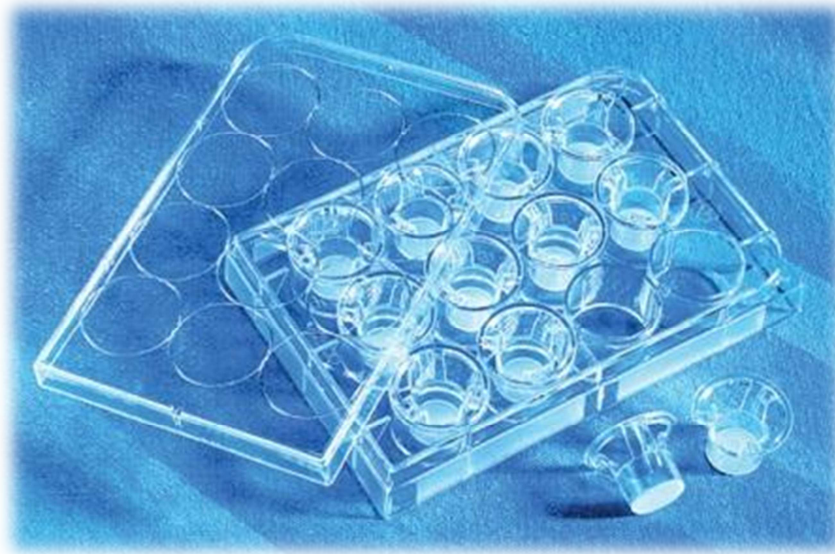


Figure 7 12mm Transwell with 0.4µm pore polycarbonate membrane insert (taken from sigmaaldrich.com)

PBECS were grown in DMEM (Dulbecco's Modified Eagle's Medium - low glucose) additionally containing 10% plasma derived bovine serum (First Link UK), 125µg/ml heparin, 2mM L-glutamine 100 U/ml Penicillin, 100µg/ml Streptomycin for 6 days at 37°C (5% CO₂). For the first 3 days, media also included 4µg/ml puromycin (an endothelial cell selection toxin). On day 6, cells were passaged. PBECS were trypsinised and pelleted before being resuspended in fresh media and plated into the transwell filter (that had been precoated with collagen and fibronectin) at a density of 1 x 10⁵ cell/cm². For non-contact co-culture, filters were then moved to 12-well plates already containing 100% confluent C6 cells. C6s (p132) were grown in DMEM (high glucose) with 10% foetal calf serum 100 U/ml Penicillin, 100µg/ml Streptomycin. C6 were defrosted directly to plates at a density of 1 x 10⁵ cell/cm² and grew to

confluence after 2 days in culture. The media was changed after these 2 days, which was one day prior to the passaging of the PBECs.

Alternatively, for contact co-culture, C6s were defrosted to the underside of the Transwell filter (precoated with collagen and fibronectin) and allowed to attach for 30 minutes, then the transwell filters were placed in 12 well plates with C6 media, where C6 media was also added to the top-side of the filter to prevent coating from drying. These C6-filters were placed at 37°C (5% CO₂) for 1 day before PBECs were seeded into the top of the filter (after the astrocyte media had been removed).

The PBECs were left in co-culture with the C6s for 3 days, before the media was changed to serum free media (DMEM-low glucose, 550nM hydrocortisone, 125µg/ml heparin, 2mM L-glutamine 100 U/ml Penicillin, 100µg/ml Streptomycin, with 250µM CPT-cAMP, 17.5µM RO-20-1724 (Calbiochem)).

TEER measurements were taken with STX100 probe, and EVOM to determine the tightness of the endothelial cells' TJs, 24 hours after serum-free media was added.

1.1.1 Permeability assay

Permeability assays were conducted in assay buffer consisting of Hank's Buffered Salt Solution (HBSS), 25 mM 4-(2-hydroxyethyl)-1-piperazineethanesulfonic acid (HEPES) and 0.1% (v/v) bovine serum albumin (BSA), which was adjusted to pH 7.4. Solutions of the HPOs (800 µM in assay buffer containing 7.5 µg/mL sodium fluorescein) were also used. The solutions were heated up to 37°C and kept in the dark, since NaF is light sensitive. The media was removed from the Transwells containing the endothelial cells and the filters were moved to a new 12-well plate, where the bottom chamber (basolateral side) already contained 1.5 mL of the warm assay buffer. 500µL of the HPO solutions were added to the top chamber (apical side) of the filter insert and shaken at 200 rpm in an orbital shaker at 37°C and in the dark. After 60 minutes the filter inserts were transferred into a new 12-well plate in order to take prevent any transport into the bottom chamber. Then the whole volume of both chambers was taken into Eppendorf tubes[®] and frozen until HPLC analysis. The filter inserts were washed with phosphate-buffered saline (PBS) (3x) and then lysed with deionized H₂O as detailed below.

1.1.2 Sodium fluorescein – paracellular marker

Besides TEER measurement, the paracellular marker sodium fluorescein was used to determine the tightness of the junctions formed between the PBEC. The dye sodium fluorescein is not able to penetrate into endothelial cells; therefore its only way from the apical to the basolateral side is the paracellular route. Measuring the amount of NaF in the basolateral chamber is an indicator of the tightness of the tight junctions.



Figure 8 - 96 well plate (taken from phenixresearch.com)

In order to determine the concentration of sodium fluorescein, a standard curve with different concentrations had to be generated. 100 μ L samples of the 800 μ M HPO solutions were pipetted into a black 96-well plate (Figure 8) at different concentrations (100%, 25%, 5%, 1%, 0.20% and 0.05%). Moreover samples from each apical and basolateral chamber were pipetted into the plate, as well as the assay buffer as a blank. Sodium fluorescein is light sensitive; hence the plate had to be covered in foil to obtain accurate results. Fluorescence was measured at an absorption maximum of 494 nm and emission maximum of 521 nm, to generate a concentration curve of sodium fluorescein and determine the amount of the paracellular marker in the samples. These results were used to correct the HPO concentrations obtained from the HPLC-data. The measurements of the sodium fluorescein transfer were used to determine the percentage of HPO transfer via the paracellular route and subtracted from the overall transfer, which was measured by HPLC.

3.2.2 Protein assay

In order to determine the intracellular accumulation of the HPOs, a protein assay was performed. After the filters had been washed with PBS (3x) and the inserts transferred into a new 12-well plate, 500 μ L water was added to each well in order to lyse the cells. The plate was stored at 37°C for 45 minutes. Then a cell scraper was used to scrape off the cells and the volume was pipetted into Eppendorf tubes[®]. Then TCA was added to the samples in order to precipitate any protein. The tubes were incubated at 4°C for 10 minutes and protein was pelleted by centrifugation in microfuge at 10,000 x g for 5 minutes. The supernatant was then collected for HPLC analysis to determine the amount of HPO maintained intracellularly within the cells.

3.2.3 HPLC system

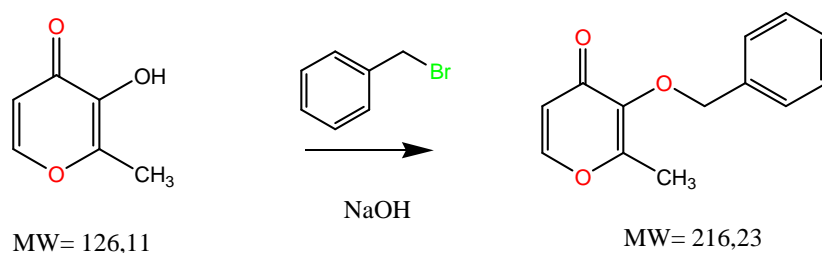
A gradient ion-pair HPLC method was used to analyse the HPOs in this study. The HPLC system consisted of an autosampler, a controller, a pump, a photodiode array detector and a reversed phase polymer column. The buffer and acetonitrile were degassed. A linear gradient of 2-35% of acetonitrile over 20 minutes was followed by a post run period of 5 minutes using 2% acetonitrile and 98% buffer. The buffer (1-heptanesulfonic acid (sodium salt), 5mM in HPLC water) was adjusted to pH 2 using HCl. The injection volume was set to 100 μ L. The flow rate was 1 mL/min and the compounds were monitored at 280 nm (Liu, Liu et al. 1999). The HPLC chromatograms were produced and analysed by using Millenium 32 software.

3.2.4 Statistical analysis

Statistical analysis was performed using GraphPad Prism software.

4 Synthetic schemes

4.1 Synthesis of 2-methyl-3-benzyloxy-pyran-4(1H)-one



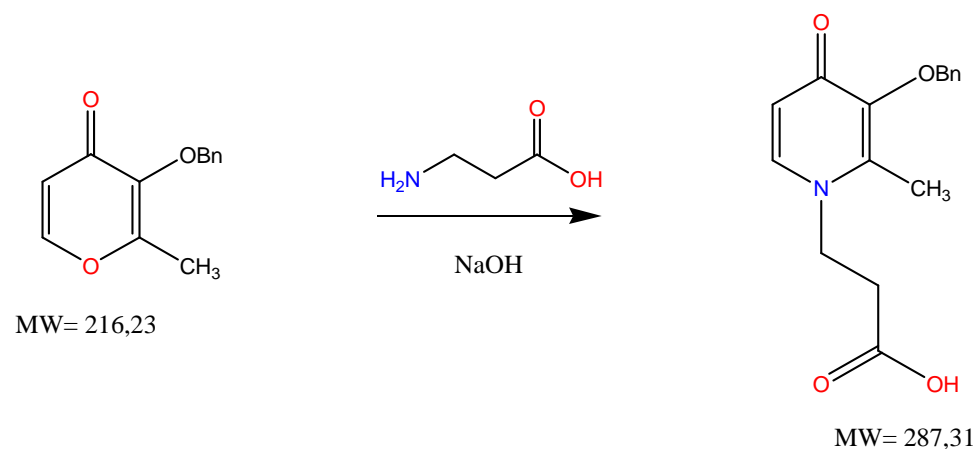
Scheme 1 Synthesis of 2-methyl-3-benzyloxy-pyran-4(1H)-one

The starting material for the synthesis of the desired iron chelator was 2-methyl-3-hydroxy-4H-pyran-4-one (maltol), as shown in Scheme 1. The initial step was the protection of the hydroxyl group of maltol by benzylation. Applying the Williamson ether synthesis method, the starting material was treated with sodium hydroxide to generate the nucleophilic alkoxide. Then the alkyl halide benzyl bromide was added dropwise and the mixture refluxed overnight. Thus the nucleophilic alkoxide could attack the electrophilic carbon atom of the benzyl bromide and the desired benzyl ether was formed via an S_N2 mechanism. After removal of the solvent under reduced pressure, the residue was dissolved in dichloromethane and washed with 5% aqueous sodium hydroxide followed by water. The organic layer was dried, filtered and rotary evaporated. Re-crystallization from diethyl ether afforded crystals in an acceptable yield, after the solution was allowed to stand in the fridge overnight.

The presence of the protective benzyl group was proved by the results from the ¹H – nuclear magnetic resonance (¹H - NMR) investigation. Deuterated methanol (MeOD) was used to dissolve the crystals for the ¹H – NMR spectra. The hydrogen atoms from the CH₂-group of the benzyl group appeared as a singlet at a chemical shift of 5.08 parts per million (ppm) whereas the aromatic hydrogen atoms showed a multiplet at δ 7.33 – 7.41.

The detailed synthetic procedure is described in section 5.1.

4.2 Synthesis of 1-(2'-carboxyethyl)-2-methyl-3-(benzyloxy)-4(1H)-pyridinone



Scheme 2 Synthesis of 1-(2'-carboxyethyl)-2-methyl-3-(benzyloxy)-4(1H)-pyridinone

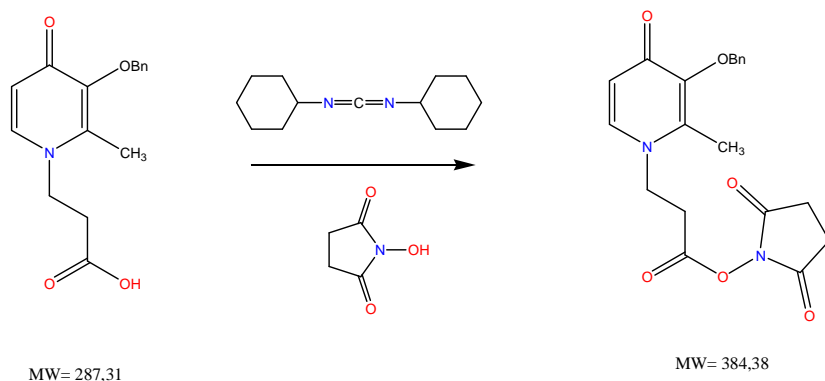
The previously prepared benzyl-protected maltol can be converted into the 4-pyridinone-derivative through an amine insertion reaction. The reaction starts with an aza-Michael-addition at the alpha, beta unsaturated ketone. The nucleophilic primary amine targets the oxygen in the 4-pyrone, the ring is hence opened and a molecule of water is eliminated. Thereafter, the ring closes again and the desired 4-pyridinone is generated. (Elkaschef 1960)

To convert the 4-pyrone into the desired 4-pyridone, β -alanine (3-aminopropionic acid) was added to the starting material. The pH was adjusted to 13 with NaOH and the mixture refluxed for 18 hours. Then the solution was reduced in volume and the pH acidified to 4, which led to a fluffy precipitation. This fluffy precipitate was extracted from the aqueous phase into DCM and the organic layer was filtered to yield a yellow powder. The powder was dissolved in the smallest possible amount of ethanol and then diethyl ether was added dropwise until the appearance of a slight cloudiness. The flask was stored at 4° C overnight to gain an acceptable yield of a slightly yellow powder.

The structure was investigated by $^1\text{H-NMR}$ and the four protons of the carboxyethyl-moiety were observed at δ 2.58-2.61 and 4.13-4.16 ppm. The carboxylic proton could not be seen, because it dissociated in the solvent, MeOD. The protons of the pyridinone-derivative were found at chemical shifts as follows: δ 2.10 (3H, s, CH_3), 4.96 (2H, s, CH_2Ph), 6.36-6.38 (1H, d, **5-H**), 7.21-7.30 (5H, m, CH_2Ph), 7.65-7.67 (1H, d, **6-H**).

The detailed synthetic procedure is described in section 5.2.

4.3 Synthesis of 1-[2'-[(succinimidyl)oxy]carbonyl]ethyl)-2-methyl-3-benzyloxy-4(1H)-pyridinone



Scheme 3 Synthesis of 1-[2'-[(succinimidyl)oxy]carbonyl]ethyl)-2-methyl-3-benzyloxy-4(1H)-pyridinone

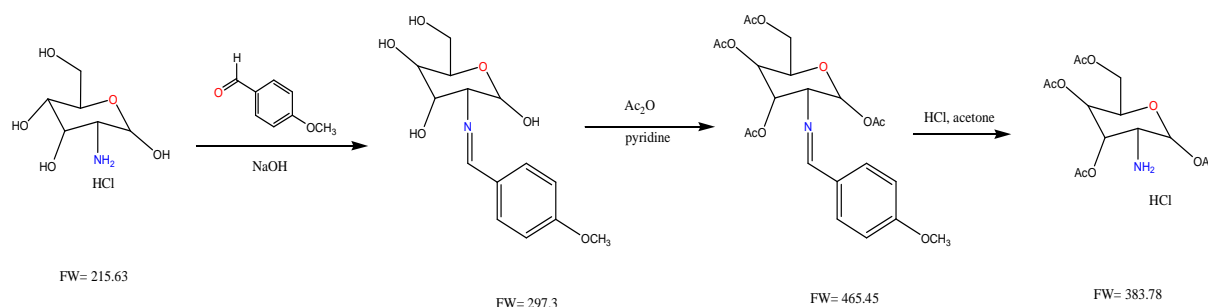
Applying the Steglich esterification method, the carboxylic acid group is treated with a coupling reagent, dicyclohexylcarbodiimide (DCC), and N-hydroxysuccinimide (NHS). DCC reacts with the starting material and forms a highly unstable active O-acylisourea intermediate. The activated acid intermediate reacts with NHS forming the NHS-ester. (Neises and Steglich 1978; Hermanson 2008) [2]

In order to generate the NHS-ester, the starting material was dissolved in dry DMF. DCC and NHS, also dissolved in DMF, were added and the solution stirred at room temperature for 18 hours. The mixture was filtered to remove dicyclohexylurea (DCU), a hardly soluble by-product and concentrated under reduced pressure to give a white solid. The product was stored in a desiccator to prevent hydrolysis of the NHS-ester.

¹H-NMR – investigation proved the presence of the additional four protons of the NHS-ester-moiety. The protons appeared as a singlet at a chemical shift of 2.74 ppm.

The detailed synthetic procedure is described in section 5.3.

4.4 Synthesis of 1,3,4,6-tetra-O-acetyl- β -D-glucosamine hydrochloride



Scheme 4 Synthesis of 1,3,4,6-tetra-O-acetyl- β -D-glucosamine hydrochloride

For the synthesis of the desired iron chelator the glucosamine had to be selectively protected. First the amino group of the glucosamine is treated with anisaldehyde, to form the protective enamine, before acetylation. Acetic anhydride and pyridine were added to convert the hydroxyl groups into acetic acid esters. In the last step, the *p*-methoxybenzylidene group was removed with aqueous HCl to afford the desired 1,3,4,6-tetra-O-acetyl- β -D-glucosamine hydrochloride.

Glucosamine hydrochloride was dissolved in NaOH and treated with *p*-anisaldehyde. After stirring the solution was stored at room temperature, which lead to the formation of a crystal mass. The flask was stored at 4°C overnight. The crystal mass was collected on a Büchner funnel and washed with cold water followed by ether to yield the *p*-methoxybenzylidene derivative.

Acetylation was performed under cooling by the addition of acetic anhydride and pyridine. The mixture was stored at room temperature for 24 hours and then poured into ice-cold water. The precipitate was filtered off to yield the *N*-[*p*-methoxybenzylidene]-tetraacetyl-D-glucosamine.

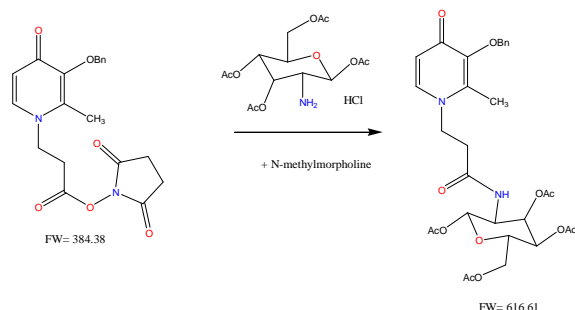
In order to remove the *p*-methoxybenzylidene group, the protected glucosamine was dissolved in acetone and heated until boiling. After the addition of aqueous HCl precipitation of the glucosamine hydrochloride was observed. After cooling, ether was added and flask stored at 4°C. The crystals were collected on a Büchner funnel and washed with cold ether. Re-crystallization from MeOH afforded the desired glucosamine derivative.

¹H-NMR investigation confirmed the structure of the sugar and all signals of the protons could be assigned. δ 5.95-5.97 (1H, d, **1**-H), 5.45-5.50 (1H, m, **3**-H), 5.12-5.17 (1H, m, **4**-H), 4.37-4.40 (1H, m, **6a**-H), 4.20-4.24 (1H, m, **6b**-H), 3.93 (1H,

s, **5-H**), 3.71-3.76 (1H, m, **2-H**), 2.10 (3H, s, **CH₃**), 2.11 (3H, s, **CH₃**), 2.15 (3H, s, **CH₃**), 2.23 (3H, s, **CH₃**).

The detailed synthetic procedure will be described in section 5.4.

4.5 Synthesis of N-(1,3,4,6-tetra-O-acetyl-2-deoxy-β-D-glucopyranos-2-yl)-3-(3-(benzyloxy)-2-methyl-4-oxopyridin-1(4H)-yl)propanamide



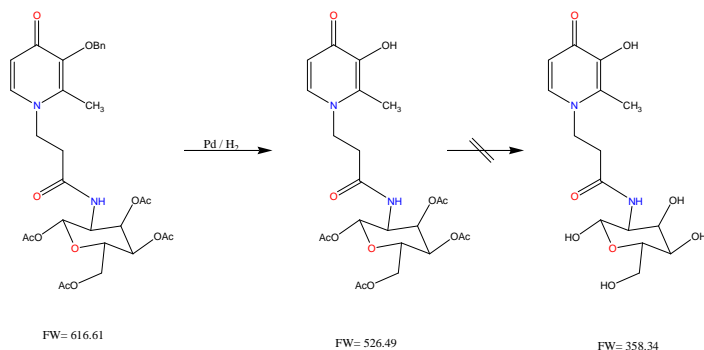
Scheme 5 Synthesis of N-(1,3,4,6-tetra-O-acetyl-2-deoxy-β-D-glucopyranos-2-yl)-3-(3-(benzyloxy)-2-methyl-4-oxopyridin-1(4H)-yl)propanamide

Scheme 5 demonstrates the synthesis of the desired compound, by forming an amide bond between the activated ester and a primary amine. 1,3,4,6-tetra-O-acetyl glucosamine cannot react with the carboxylic acid directly, because it is a weak nucleophile. Therefore the carboxylic acid had been converted into the active ester, which is more prone to react with nucleophiles. Under mild conditions the primary amine reacts with the NHS-ester to form a stable amide bond. N-hydroxysuccinimide is released and a molecule of water is eliminated. (Montalbetti and Falque 2005; Hermanson 2008)

The starting material, 1-[2'-[(succinimidyl)oxy]carbonyl]ethyl)-2-methyl-3-benzyloxy)-4(1H)-pyridinone, was dissolved in DMF/water (9:1) and N-methylmorpholine was added. 1,3,4,6-tetra-O-acetyl glucosamine was dissolved in DMF/water (9:1) and added dropwise. The solution was stirred at room temperature for 14 hours. Afterwards, the solution was poured into water and stirred for 30 minutes. The mixture was filtered and the filtrate dried by rotary evaporation to give an off-white solid. In order to remove the by-products the residue was taken up in DCM and washed with aqueous acetic acid, followed by water and aqueous bicarbonate solution. The organic fractions were collected and dried over anhydrous Na₂SO₄. After the sodium sulfate had been filtered off, the filtrate was dried by rotary evaporation to yield a dark residue. ¹H-NMR investigation confirmed the presence of the desired compound. In addition to the peaks of the pyridinone-derivate the protons of the acetyl-groups appeared as four singlet peaks at the chemical shifts of 2.00, 2.02, 2.07 and 2.13.

The detailed synthetic procedure is described in section 5.5.

4.6 Deprotection of N-(1,3,4,6-tetra-O-acetyl-2-deoxy-β-D-glucopyranos-2-yl)-3-(3-(benzyloxy)-2-methyl-4-oxopyridin-1(4H)-yl)propanamide



Scheme 6 Deprotection of N-(1,3,4,6-tetra-O-acetyl-2-deoxy-β-D-glucopyranos-2-yl)-3-(3-(benzyloxy)-2-methyl-4-oxopyridin-1(4H)-yl)propanamide

To generate the desired iron chelator the protective groups, benzyl ether and acetic acid ester, had to be eliminated. Deprotection of the benzyl ether was performed as a palladium-catalysed hydrogenation, delivering the phenol and toluene. The protected iron chelator was dissolved in EtOH (100 mL) and palladium (5% water, on calcium carbonate, dosed with lead) was added. Hydrogenation was carried out at 40 psi overnight. The reaction was completed within 24 hours. After the catalyst had been filtered off, the solvent was removed under reduced pressure to yield 200 mg of a hard film. The reaction was monitored by TLC (DCM / MeOH 9:1).

In order to remove the acetyl groups the residue was taken up in CHCl_3 . An aliquot was taken and the solvent, CHCl_3 , dried by rotary evaporation. The remaining solid was dissolved in DMSO and a 100 mM NaOD-solution was prepared using sodium metal and D_2O . Deuterated solvent was used to monitor the process of the reaction directly by NMR-investigation. 1 mL of this solution was added to the flask and the sample was analysed by $^1\text{H-NMR}$ at different points of time in order to investigate when the cleavage of the acetyl groups was completed. Measurements were carried out after 5, 40 and 100 minutes. Analysis of the NMR spectra showed that the reaction was very fast, because the signals of the acetyl groups were decreased after 5 minutes. There was no significant change between the spectra taken at later points of time. This confirms that a 100 mM NaOH-solution is sufficient to eliminate the acetic acid esters.

These steps were repeated with the remaining residue. The content of the flask was dissolved in DMSO and a 100 mM NaOH solution was added. The flask was stored at room temperature for one hour. Then deionized water was added and the pH neutralized to 7 with aqueous HCl. After extraction into CHCl_3 , the organic layer was dried over Na_2SO_4 and filtered. The solvent was removed under reduced pressure to yield 14 mg of a white residue. $^1\text{H-NMR}$ analysis showed lack of the desired product. The spectrum contained only peaks of the solvent (DMSO). Therefore, the aqueous phase was saturated with NaCl in order to reduce the solubility of the compound in water and placed in a separating funnel. Chloroform was added and the funnel shook several times over ten minutes. The organic layer was dried over Na_2SO_4 , filtered and dried by rotary evaporation to yield a colourless film. NMR investigation showed again lack of the desired compound.

The conditions of the deprotection need to be investigated further. A possible way could be to remove the acetyl groups first. In this order the molecule stays more hydrophobic and it should be extracted more easily into CHCl_3 . Then the cleavage of the benzyl ether could be performed by hydrogenation.

Unfortunately, the protected iron chelator was used up and due to the limited time that was available for my project the deprotection could not be repeated.

5 Synthetic procedures

5.1 Synthesis of 2-methyl-3-benzyloxy-pyran-4(1H)-one

The procedure of this synthesis was taken from J. Med. Chem. 1993, 36, 2448 – 2458: *Synthesis, Physicochemical Properties, and Biological Evaluation of N-substituted 2-Alkyl-3-hydroxy-4(1H)-pyridinones: Orally Active Iron Chelators with Clinical Potential*(Gaeta, Molina-Holgado et al. 2011)

Maltol (25.0011 g; 198.24 mmol) was dissolved in 250 mL MeOH in a two-neck round bottomed flask, equipped with a magnetic stirrer. A solution of NaOH (8.48 g) in 30 mL water was added. Then benzyl bromide (25.3 mL; 212.4 mmol) was added dropwise through an addition funnel to the stirred solution. The bath temperature was adjusted to 70° Celsius and the mixture was refluxed overnight. During the night the colour of the clear solution turned to dark orange. On the next day the completion of the reaction was checked by TLC (hexane / ethyl acetate 1:1). The solvent (MeOH) was removed under reduced pressure. The residue was dissolved in 100 mL DCM and placed in a separating funnel. The solution was washed first with 5% sodium hydroxide (2x 100 mL) followed by water (2x 100 mL). The organic layer was dried over anhydrous sodium sulfate, filtered and the solvent removed under reduced pressure to yield an oil which solidified on cooling. Re-crystallization from diethyl ether afforded off-white crystals and the flask was stored at 4° C overnight. The next day the crystal mass was filtered and washed with cold diethyl ether to gain white crystals; **yield:** 50%. **Melting point:** 54-55° C. **¹H-NMR (MeOD):** δ 2.12 (3H, s, CH₃), 5.08 (2H, s, CH₂Ph), 6.41-6.42 (1H, d, **5**-H), 7.33-7.41 (5H, m, CH₂Ph), 7.93-7.94 (1H, d, **6**-H).

5.2 Synthesis of 1-(2'-carboxyethyl)-2-methyl-3-(benzyloxy)-4(1H)-pyridinone

The procedure of this synthesis was taken from J. Med. Chem. 1993, 36, 2448 – 2458: *Synthesis, Physicochemical Properties, and Biological Evaluation of N-substituted 2-Alkyl-3-hydroxy-4(1H)-pyridinones: Orally Active Iron Chelators with Clinical Potential*(Gaeta, Molina-Holgado et al. 2011)

To a solution of 2-methyl-3-(benzyloxy)-4(4H)-pyranone (5.4014 g; 25 mmol) in ethanol (63 mL) in a round bottomed flask containing a magnetic stirrer was added β -alanine (2.6060 g; 30 mmol) dissolved in water (63 mL). 10 N sodium hydroxide solution was used to adjust the pH to 13. The mixture was refluxed overnight at a bath temperature of 100° C. After 18 hours of reflux the clear solution had turned dark orange. The reaction was monitored by TLC (ethyl acetate / acetic acid 9:1). The solution was reduced in volume and the pH adjusted to 4, using 5N HCl. The residue was extracted into DCM (3x 50 mL) and the organic layer dried over sodium sulfate. After the sodium sulfate was filtered off, the solvent was removed under reduced pressure to afford crystals. The residue was dissolved in the smallest possible amount of ethanol and then diethyl ether was added slowly until the appearance of a slightly cloudiness. The mixture was stored at 4° C overnight. The precipitate was filtered and washed with cold ether. Yellow crystals were obtained in 50% yield. **MP:** 170-171° C. **¹H-NMR (MeOD):** δ 2.10 (3H, s, CH₃), 2.58-2.62 (2H, m, N-CH₂-CH₂-), 4.13-4.17 (2H, m, N-CH₂-CH₂-), 4.96 (2H, s, CH₂Ph), 6.36-6.38 (1H, d, 5-H), 7.21-7.30 (5H, m, CH₂Ph), 7.66-7.67 (1H, d, 6-H).

The reaction was repeated with the aim of increasing the yield. To a solution of 2-methyl-3-(benzyloxy)-4(4H)-pyranone (10 g; 48 mmol) in ethanol (120 mL) was added β -alanine (5 g; 56 mmol) dissolved in water (120 mL). The pH was adjusted to 13 with 10 N NaOH and the mixture refluxed for 18 hours. The reaction was monitored by TLC (EtOAc / acetic acid 9:1). The mixture was reduced in volume by rotary evaporation and the remaining solution was acidified with HCl to pH 4. A change in colour from clear to dark yellow and precipitation was observed. DCM was added to wash the aqueous phase (3x 100 mL). The precipitate was collected on a

Büchner funnel and dried over vacuum. $^1\text{H-NMR}$ investigation of this yellow precipitate confirmed the structure and showed that the product was sufficiently pure for synthetic use. Yield was increased to 70%. MP: 170-171° C. $^1\text{H-NMR (MeOD)}$: δ 2.10 (3H, s, CH_3), 2.58-2.61 (2H, m, N- $\text{CH}_2\text{-CH}_2\text{-}$), 4.13-4.16 (2H, m, N- $\text{CH}_2\text{-CH}_2\text{-}$), 4.96 (2H, s, CH_2Ph), 6.36-6.38 (1H, d, **5-H**), 7.21-7.30 (5H, m, CH_2Ph), 7.65-7.67 (1H, d, **6-H**). $^{13}\text{C-NMR (MeOD)}$: δ 12.80 (CH_3), 35.43 (N- $\text{CH}_2\text{-CH}_2\text{-}$), 50.90 (N- $\text{CH}_2\text{-CH}_2\text{-}$), 74.60 (CH_2Ph), 117.17 (**5-C**), 129.39+129.45+130.29+138.41 (CH_2Ph), 141.62 (**6-C**), 145.34 (**2-C**), 147.02 (**3-C**), 173.51 (N- $\text{CH}_2\text{-CH}_2\text{-COOH}$), 174.70 (**4-C**).

5.3 Synthesis of 1-[2'-[(succinimidyloxy)carbonyl]ethyl]-2-methyl-3-benzyloxy)-4(1H)-pyridinone

The procedure of this synthesis was taken from J. Med. Chem. 1993, 36, 2448 – 2458: *Synthesis, Physicochemical Properties, and Biological Evaluation of N-substituted 2-Alkyl-3-hydroxy-4(1H)-pyridinones: Orally Active Iron Chelators with Clinical Potential*(Gaeta, Molina-Holgado et al. 2011)

This section will describe different approaches to synthesize 1-[2'-[(succinimidyloxy)carbonyl]ethyl)-2-methyl-3-benzyloxy)-4(1H)-pyridinone since some difficulties were experienced and the conditions of this reaction had to be more carefully defined.

In the first attempt the 1-(2'-carboxyethyl)-2-methyl-3-(benzyloxy)-4(1H)-pyridinone (0.5752 g; 2 mmol) and NHS (0.2312 g; 2 mmol) were dissolved in DMF (20 mL). After the addition of DCC (0.4137 g; 2 mmol) the solution was stirred at room temperature for 18 hours. The reaction was monitored by TLC (EtOAc / ACN / MeOH 2:2:1). The solution was filtered in order to remove DCU and the solvent was evaporated under reduced pressure to yield a light yellow solid. The residue was dissolved in the smallest possible amount of DCM followed by ether. After the addition of ether some crystals started to form immediately, so the flask was stored overnight at room temperature. On the next day the amount of crystals was very low and the flask contained some oily remains. The solvents (DCM / ether) were removed under reduced pressure in order to try the re-crystallization again. This time the flask was left in the fridge overnight, however the yield of the crystals remained low. The solid was separated from the oily phase and both samples were taken for ¹H-NMR investigation. The NMR-spectra showed lack of the desired compound. The signals of the chemical shifts could be assigned to the reactants.

In the second attempt two equivalents of DCC were used. The conditions and the amount of the other reactants were retained. The solution was stirred for 18 hours and filtered. The reaction as monitored by TLC (EtOAc / ACN / MeOH 2:2:1). The solvent was removed under reduced pressure and DCM was added. Unfortunately, the mixture did not become clear, despite adding large amounts of DCM, so re-crystallization was impossible. By using a different mobile phase (CHCl₃ /

MeOH 4:1) for the TLC the three highest spots could be separated enough for column chromatography. All fractions containing the desired spots were collected and the solvents removed by rotary evaporation. $^1\text{H-NMR}$ investigation showed again presence of the reactants and absence of the desired product. Consequently, increasing the amount of the coupling reagent does not improve the reaction.

In the next approach anhydrous DMF was used, which had been distilled on the same day. In a three-neck-flask 2 mmol of 1-(2'-carboxyethyl)-2-methyl-3-(benzyloxy)-4(1H)-pyridinone (0.57015 g) were put under vacuum followed by N_2 -flow for three times to get rid of all the air inside the flask. The other two necks of the flask were suba-sealed. Then dry DMF (12 mL) was added using a syringe to dissolve the pyridinone-derivative. The other reactants, DCC and NHS, were dissolved in DMF (3 mL each), using separate flasks and also added to the three-neck-flask through a syringe. The solution was stirred at room temperature under constant N_2 -flow for 18 hours. The presence of a white precipitate, DCU, indicated that some kind of reaction had occurred. This precipitate was filtered off and the solvent removed under reduced pressure. DCM was added to the residue in order to re-crystallize it. The solid did not dissolve completely in DCM and an excess of ether was added which led to precipitation. The flask was stored at room temperature to gain more of the precipitate. The mixture was filtered by suction and the precipitate washed with cold ether and dried under vacuum. $^1\text{H-NMR}$ investigation proved the presence of the desired compound, by showing the additional four protons of the NHS-ester-moiety at a chemical shift of 2.74 ppm.

However, the NMR-spectrum contained some impurities, and so the sample was subjected to re-crystallization. 100 mg of the solid were dissolved in DCM (3 mL) and heated. This mixture was filtered and then an excess of ether was added to the filtrate. Some crystals formed and the flask was stored at 4° C. The mixture was filtered and the mother liquor was removed under reduced pressure to yield 20 mg of crystals. $^1\text{H-NMR}$ investigation showed a spectrum with even more impurities. Maybe the product hydrolysed partly during the process of re-crystallization. This crude product was used for the next reaction. **Yield:** 77%. **MP:** 144 - 147° C. **$^1\text{H-NMR}$ (MeOD):** δ 2.10 (3H, s, CH_3), 2.74 (4H, s, $\text{N-C(=O)-CH}_2\text{-CH}_2\text{-C(=O)}$), 2.99-3.02 (2H, m, $\text{N-CH}_2\text{-CH}_2\text{-}$), 4.26-4.29 (2H, m, $\text{N-CH}_2\text{-CH}_2\text{-}$), 4.96 (2H, s, CH_2Ph), 6.34-6.36 (1H, d, 5-H), 7.22-7.31 (5H, m, CH_2Ph), 7.66-7.67 (1H, d, 6-H). **$^{13}\text{C-NMR}$ (MeOD):** δ 12.77 (CH_3), 26.09 ($\text{N-C(=O)-CH}_2\text{-CH}_2\text{-C(=O)}$), 32.51 ($\text{N-CH}_2\text{-CH}_2\text{-}$), 49.92 ($\text{N-CH}_2\text{-CH}_2\text{-}$),

74.63 (**CH₂Ph**), 117.46 (**5-C**), 129.39+129.47+130.34+138.42 (**CH₂Ph**), 141.63 (**6-C**), 145.12 (**2-C**), 147.15 (**3-C**), 167.76 (N-CH₂-CH₂-COO-), 171.56 (N-C(=O)-CH₂-CH₂-C(=O)), 175.16 (**4-C**)

In order to investigate the conditions of this reaction further the reaction was performed without N₂-flow. The reactants were dissolved in anhydrous DMF in three separate flasks, which had been washed with acetone, dried in an oven and then stored in a desiccator. 1-(2'-Carboxyethyl)-2-methyl-3-(benzyloxy)-4(1H)-pyridinone (0.9987 g) was dissolved in 20 mL DMF in a round bottomed flask and suba-sealed. NHS (0,426 g) and DCC (0.718 g) were dissolved in DMF (5 mL each) and added to the round bottomed flask using a syringe. The mixture was stirred at room temperature overnight and the flask additionally covered with parafilm. DCU precipitated and indicated that some kind of reaction did occur. The precipitate was collected on a Büchner funnel and the filtrate evaporated to yield a off-white solid. The residue was investigated by ¹H-NMR spectroscopy. The NMR-spectrum shows the four protons of the NHS-ester, but again impurities of around 30%. The additional peaks could be assigned to 1-(2'-carboxyethyl)-2-methyl-3-(benzyloxy)-4(1H)-pyridinone, starting material that did not react. **Yield:** 77 %. **MP:** 144 - 146° C. **¹H-NMR (DMSO):** δ 2.23 (3H, s, CH₃), 2.82 (4H, s, N-C(=O)-CH₂-CH₂-C(=O)), 3.189-3.21 (2H, m, N-CH₂-CH₂-), 4.22-4.26 (2H, m, N-CH₂-CH₂-), 5.0 (2H, s, CH₂Ph), 6.14-6.15 (1H, d, **5-H**), 7.31-7.43 (5H, m, CH₂Ph), 7.66-7.67 (1H, d, **6-H**).

To gain an acceptable yield of the NHS-ester, the reaction does not have to be performed under N₂-flow. The use of dry DMF is essential, because the active ester is labile to hydrolysis. Therefore anhydrous conditions are very important and the product should be stored in a desiccator in order to prevent it from decomposition.

5.4 Synthesis of 1,3,4,6-tetra-O-acetyl- β -D-glucosamine hydrochloride

The procedure of this synthesis was taken from Eur. J. of inorganic Chem. 1964, 64, 978: *Synthesen mit Glucosamin*. (Bergmann and Zervas 1964)

To synthesize the desired iron chelator a selectively protected glucosamine had to be prepared. Following the instructions of the paper, the glucosamine hydrochloride (10 g) was dissolved in 1N NaOH (47 mL). Then p-anisaldehyde (5.7 mL) was added and the solution stirred well. When the flask was stored at room temperature crystals began to form and the flask was stored at 4° C overnight. The crystal mass was collected on a Büchner funnel and washed with ice-cold water followed by ether to yield 69% of the N-protected p-methoxybenzylidene derivative. The product was dried under vacuum.

In the next step a part of the N-protected sugar (5.0197 g) was dissolved with cooling in a mixture of acetic anhydride (15 mL) and dry pyridine (27 mL). The solution was stirred for 30 minutes and then the flask was stored at room temperature over 48 hours. Afterwards the mixture was poured into ice-cold water and the precipitate filtered off. The acetylated product was dried over vacuum to afford 70% of crystals.

In the last step the protected glucosamine is treated with HCl in order to remove the p-methoxybenzylidene group. The protected sugar (4.9996 g) was dissolved in the smallest possible amount of acetone and refluxed. Addition of 1 equivalent of 5N HCl (2 mL) led to immediate precipitation of the hydrochloride derivative. After cooling, the solid was broken up and ether (5 mL) was added. The mixture was stirred for 30 minutes and then the flask was stored at 4° C overnight. The precipitate was filtered off and washed with ice-cold ether. The crystals were dried in a desiccator. White crystals were obtained in 90% yield. NMR investigation confirmed the structure of 1,3,4,6-tetra-O-acetyl- β -D-glucosamine hydrochloride. **MP:** > 230 °C: becomes dark without melting. **¹H-NMR (D₂O):** δ 5.95-5.97 (1H, d, **1-H**), 5.45-5.50 (1H, m, **3-H**), 5.12-5.17 (1H, m, **4-H**), 4.37-4.40 (1H, m, **6a-H**), 4.20-4.24 (1H, m, **6b-H**), 3.93 (1H, s, **5-H**), 3.71-3.76 (1H, m, **2-H**), 2.10 (3H, s, **CH₃**), 2.11 (3H, s, **CH₃**), 2.15 (3H, s, **CH₃**), 2.23 (3H, s, **CH₃**). **¹³C-NMR (D₂O):** δ 19.96 (O=C-**CH₃**), 20.0 (O=C-**CH₃**), 20.13 (O=C-**CH₃**), 52.37 (**2-C**), 61.38 (**6-C**), 67.97 (**4-C**), 71.05 (**3-**

C), 72.07 (**5-C**), 90.60 (**1-C**), 171.21 (O=C-CH₃), 172.66 (O=C-CH₃), 172.99 (O=C-CH₃), 173.52 (O=C-CH₃).

The preparation of 1,3,4,6-tetra-O-acetyl- β -D-glucosamine hydrochloride was repeated with benzaldehyde to gain more material for the following coupling reaction. To a solution of glucosamine hydrochloride (10 g) in 1N NaOH (47 mL) was added benzaldehyde (6 mL). The solution was stirred for 30 minutes and the flask stored at 4° C overnight. In contrast to the reaction with p-anisaldehyde there was no precipitate. The solution was placed in a separating funnel and ethyl acetate (50 mL) was added. Precipitation of white flakes occurred immediately. The precipitate was collected on a Büchner funnel and dried over vacuum. ¹H-NMR investigation proved presence of the N-protected glucosamine. Yield: 45%.

A part of the N-protected sugar (5.0048 g) was taken up in a mixture of acetic anhydride (15 mL) and dry pyridine (27 mL) under cooling. The solution was stirred for 30 minutes and then the flask was stored at room temperature over 48 hours. The mixture was poured into ice-cold water and the precipitate filtered by suction to yield 57%.

The smallest possible amount of acetone was used to dissolve the acetylated intermediate (3.9994) and refluxed. After the addition of 1 equivalent of 5N HCl the solution solidified immediately. The mass was broken up after cooling. Diethyl ether was added (5 mL) and the solution stirred for 30 minutes. The flask was stored at 4° C overnight. The crystals were collected on a Büchner funnel and dried over vacuum to afford 68% of white crystals. ¹H-NMR investigation confirmed the structure of 1,3,4,6-tetra-O-acetyl- β -D-glucosamine hydrochloride. ¹H-NMR (D₂O): δ 5.94-5.96 (1H, d, **1-H**), 5.45-5.49 (1H, m, **3-H**), 5.12-5.17 (1H, m, **4-H**), 4.37-4.41 (1H, m, **6a-H**), 4.23-4.24 (1H, m, **6b-H**), 4.20-4.21 (1H, s, **5-H**), 3.71-3.75 (1H, m, **2-H**), 2.10 (3H, s, CH₃), 2.11 (3H, s, CH₃), 2.15 (3H, s, CH₃), 2.23 (3H, s, CH₃). ¹³C-NMR (D₂O): δ 19.97 (O=C-CH₃), 20.0 (O=C-CH₃), 20.13 (O=C-CH₃), 52.39 (**2-C**), 61.38 (**6-C**), 67.98 (**4-C**), 71.11 (**3-C**), 72.07 (**5-C**), 90.67 (**1-C**), 171.23 (O=C-CH₃), 172.67 (O=C-CH₃), 173.01 (O=C-CH₃), 173.52 (O=C-CH₃).

In summary, both aldehydes can be used to synthesize the desired 1,3,4,6-tetra-O-acetyl- β -D-glucosamine hydrochloride in acceptable yield. Using p-anisaldehyde the yield was 20% higher, however the NMR spectrum showed some

additional peaks. The peaks could be assigned to reactants, pyridine and p-anisaldehyde. Re-crystallization from MeOH afforded the pure 1,3,4,6-tetra-O-acetyl- β -D-glucosamine hydrochloride. The spectrum of the 2nd reaction was very clean with no additional peaks and showed that the product was sufficiently pure for synthetic use.

5.5 Synthesis of N-(1,3,4,6-tetra-O-acetyl-2-deoxy- β -D-glucopyranos-2-yl)-3-(3-(benzyloxy)-2-methyl-4-oxopyridin-1(4H)-yl)propanamide

The procedure of this synthesis was taken from Eur. J. Org. Chem. 2006, 2715 – 2722: *N-Carboxymethylated 6,7-Dimethoxy-4-trifluoromethylcarbostyrils as Fluorescence Markers for Amino Acids, Peptides, Amino Carbohydrates and Amino Polysaccharides.*(Badgujar 2006) This article describes the formation of an amide bond between a similar active ester and glucosamine hydrochloride. According to the paper a high yield of the desired amide was achieved, therefore the synthesis N-(1,3,4,6-tetra-O-acetyl-2-deoxy- β -D-glucopyranos-2-yl)-3-(3-(benzyloxy)-2-methyl-4-oxopyridin-1(4H)-yl)propanamide was performed under the same conditions.

Following the instructions of the above mentioned paper the active ester, 1-[2'-[(succinimidyl)oxy]carbonyl]ethyl)-2-methyl-3-benzyloxy)-4(1H)-pyridinone (149.5 mg; 0.39 mmol) was dissolved in DMF/water (9:1; 5.6 mL + 624 μ L) and N-methylmorpholine (43 μ L; 0.39 mmol) was added. 1,3,4,6-Tetra-O-acetyl glucosamine hydrochloride (150 mg; 0.39 mmol), dissolved in DMF/water (9:1; 5.6 mL + 624 μ L) was added dropwise. The solution was stirred at room temperature overnight. The mixture was poured then into water (45 mL) and stirred for 30 minutes. According to the paper the desired product should precipitate, but no such precipitate formed. The TLC plate of the solution showed additional spots to the starting materials, which indicated that a reaction had taken place. Bicarbonate was used to adjust the pH to 9 and the flask was stored at room temperature for 30 minutes. After extraction into EtOAc (2x 60 mL) the organic layer was dried over Na₂SO₄. The solvent was removed under reduced pressure to give a white residue. Analysing a sample of this residue by ¹H-NMR investigation demonstrated the absence of the desired product.

In the next attempt 1,3,4,6-tetra-O-acetyl glucosamine hydrochloride was converted into the free base. The sugar (248 mg) was dissolved in water (50 mL) and N-methylmorpholine (71.5 μ L) was added. The flask was stored for 10 minutes at room temperature. Then the solution was extracted into DCM (2x 25 mL), the organic fractions dried over Na₂SO₄. The active ester (286 mg) was taken up in DCM (10 mL) and filtered, to remove the undissolved residue. Both filtrates were combined and the

flask stored at room temperature for 24 hours. The reaction was monitored by TLC (EtOAc / ACN / MeOH 2:2:1). The solution was extracted into water (2x 50 mL) and the organic layer dried over Na₂SO₄ followed by filtration. The solvent was removed under reduced pressure to afford off-white crystals. Analysing a sample of this residue by MS showed the main peak at a mass-to-charge ratio (m/z) of 617.1, which confirmed the presence of the desired compound. NMR investigation showed characteristic peaks of the product. However, many peaks of uncoupled sugar were also present; thus the purification of this compound was necessary. **Yield:** 60 %. **MP:** 86 - 92° C. **MS (ESI) m/z:** 617.1.

In an attempt to obtain a more homogenous product, the reaction was repeated under slightly different conditions. The active ester (330 mg) was taken up in DCM (10 mL) and filtered. The filtrate was kept for the reaction. Then the glucosamine hydrochloride (275 mg) was dissolved in water (50 mL) and N-methylmorpholine (79 µL) was added in order to generate the free base of the sugar. After one minute the solution was extracted into DCM (2x 25 mL). The organic fraction was dried over Na₂SO₄ and filtered. Both filtrates were combined and the flask stored for three hours at room temperature. After extraction into water (2x 50 mL), the organic layer was dried over Na₂SO₄. The solvent was removed under reduced pressure to give white crystals. Analysis of the ¹H-NMR spectrum shows that the sample contains 45% of product but also 55% of uncoupled sugar. In order to purify the product DCM (15 mL) was added and the solution was washed with sodium acetate buffer (25 mM; adjusted to pH 4 with acetic acid; 2x 15 mL). Afterwards the organic phase was washed with water (1x 15 mL), dried over anhydrous sodium sulfate and reduced by rotary evaporation. Part of the residue was taken for ¹H-NMR analysis, which demonstrated a 1:1 ratio of product: sugar. The extraction was repeated, but this time the pH of the sodium acetate buffer was set to 3. After filtration and removal of the solvent the NMR-spectrum shows lack of the uncoupled sugar, thus confirming that extraction can be applied to purify the product. **Yield:** 10 %. **¹H-NMR (DMSO):** δ 1.88 (3H, s, OAc), 1.91 (3H, s, OAc), 1.97 (3H, s, OAc), 2.00 (3H, s, OAc), 2.19 (3H, s, CH₃), 3.96 (1H, d, **2-H''**), 4.03 (1H, d, **5-H''**), 4.05 (1H, d, **6b-H''**), 4.16 (1H, d, **6a-H''**), 4.86-4.91 (1H, t, **4-H''**), 4.99 (2H, s, CH₂Ph), 5.15-5.20 (1H, t, **3-H''**), 5.70 (1H, d, **1-H''**), 6.10-6.12 (1H, d, **6-H**), 7.32-7.42 (5H, m, CH₂Ph), 7.50-7.52 (1H, d, **5-H**), 8.17-8.19 (1H, d, NH).

In another attempt, 1-[2'-[(succinimidyl)oxy]carbonyl]ethyl)-2-methyl-3-benzyloxy)-4(1H)-pyridinone (1.0276 g; 2.68 mmol) was dissolved in aqueous DMF (40 mL) and N-methylmorpholine was added (256 μ L; 2.68 mmol). Then the glucosamine hydrochloride derivative (1.067g; 2.68 mmol) was dissolved in aqueous DMF (40 mL) and added dropwise through an addition funnel to the stirred solution. The solution was stirred at room temperature overnight. Afterwards the solution was poured into water (320 mL) and stirred for 30 minutes at room temperature. The mixture was filtered and the solvent removed under reduced pressure. The residue was taken up in DCM (100 mL) and washed with aqueous acetic acid (pH 5, 2x 50 mL), water (1x 50 mL) followed by bicarbonate solution (pH 8, 2x 50 mL). The organic layer was dried over Na₂SO₄, filtered and dried by rotary evaporation to yield 12% of a dark brown solid. NMR investigation confirmed the structure of the desired product. **¹H-NMR (CDCl₃):** δ 1.96 (3H, s, CH₃), 2.0 (3H, s, OAc), 2.02 (3H, s, OAc), 2.07 (3H, s, OAc), 2.13 (3H, s, OAc), 2.49-2.50 (2H, m, N-CH₂-CH₂-), 3.74 (1H, m, 2-H''), 4.01 (1H, d, 5-H''), 4.05-4.06 (2H, m, N-CH₂-CH₂-), 4.11 (1H, d, 6b-H''), 4.25 (1H, d, 6a-H''), 5.01 (1H, m, 4-H''), 5.12 (2H, s, CH₂Ph), 5.38 (1H, t, 3-H''), 5.89 (1H, d, 1-H''), 6.27-6.19 (1H, d, 6-H), 7.31-7.39 (5H, m, CH₂Ph), 7.51-7.53 (1H, d, 5-H), 8.36-8.38 (1H, d, NH). **¹³C-NMR (CDCl₃):** δ 12.41 (CH₃), 20.63 (O=C-CH₃), 20.70 (O=C-CH₃), 20.74 (O=C-CH₃), 20.91 (O=C-CH₃), 36.35 (N-CH₂-CH₂-), 53.31 (2-C''), 61.60 (6-C''), 68.19 (3-C''), 72.25 (5-C''), 72.67 (CH₂Ph), 73.18 (4-C''), 92.03 (1-C''), 116.37 (2-C), 116.70 (5-C), 128.28+ 128.45+ 128.96+ 129.0+ 137.08 (CH₂Ph), 138.85 (3-C), 145.87 (6-C), 169.10+ 169.45+ 169.61+ 170.32 (O=C-CH₃), 170.70 (N-CH₂-CH₂-CONH-), 172.93 (4-C).

6 Results

6.1 HPLC of HPOs (CP20, YMF25, YMF24, YMF16)

Before analysing samples of the BBB-experiment, samples of CP20 were run in deionized water to localize the peak and determine the quality and purity of the column. 100 μ L of CP20 was injected at a concentration of 100 μ M.

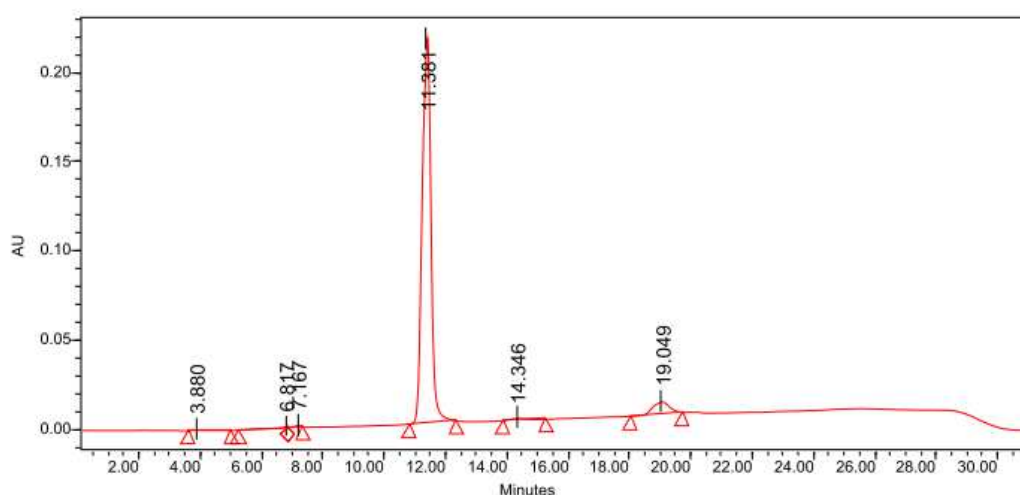


Figure 9 CP20 HPLC

100 μ L of 100 μ M CP20 from Sigma was analysed by HPLC

The chromatogram of CP20 in deionized water (Figure 9) showed a symmetrical peak at a retention time (RT) of \sim 11 minutes, but also some small additional peaks, which did not interfere with the peak of CP20. These impurities could be particles of the purified water or artefacts on the column.

Another sample of 100 μ M CP20 was run, but this time CP20 was provided by Post-Doc Yongmin Ma (Figure 10). The chromatogram showed the main peak again at RT \sim 11 minutes and impurities of the purified water.

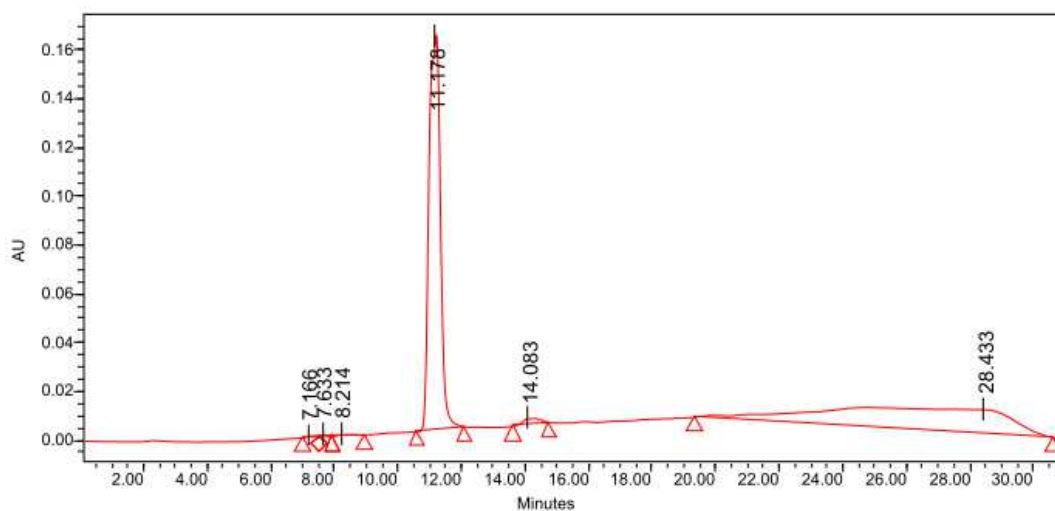


Figure 10 CP20 from Post-Doc Yongmin Ma

100 μ l of 100 μ M CP20 made by Yongmin Ma was analysed by HPLC

Therefore, CP20 from Sigma-Aldrich can be used for the experiments and for the calibration curve, since the impurities do not interfere with the RT of CP20 or with the RT of the other HPO-derivatives, YMF25, YMF24 and YMF16 (Figure 11-13).

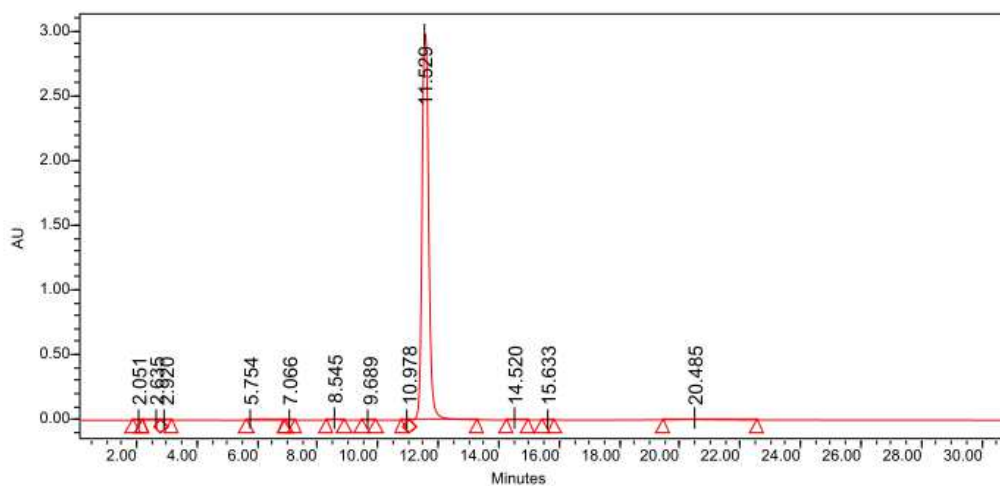


Figure 11 YMF25 800 μ M in assay buffer, RT ~ 11 minutes

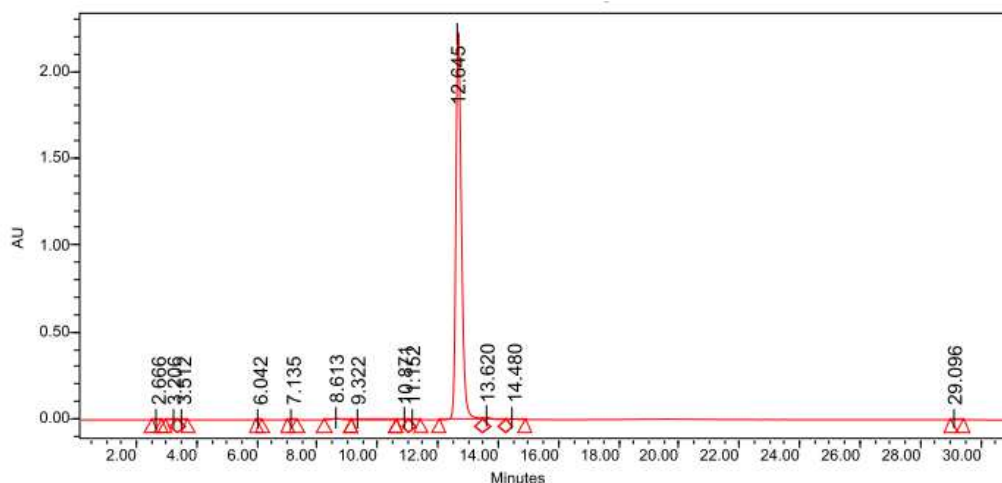


Figure 12 YMF24 800µM in assay buffer, RT ~ 12 minutes

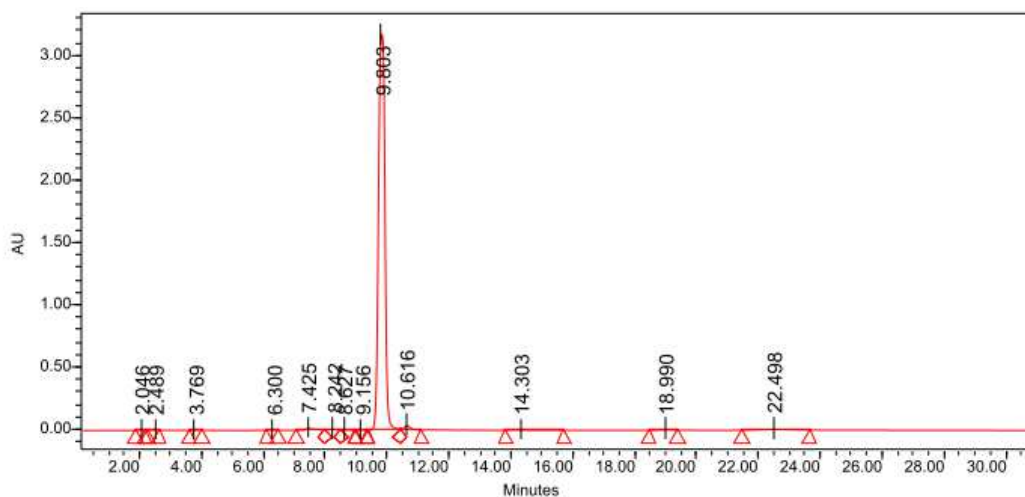


Figure 13 YMF16 800µM in assay buffer, RT ~ 10 minutes

6.2 Calibration curve – CP20

In order to quantify the amount of CP20 and the other HPOs in an unknown sample, a calibration curve was made using 100 µL injections of increasing concentrations (2.5-1000 µM) of CP20 in deionized water. The standard calibration curve for the HPOs was produced by running samples in triplicates and integrating the area under the curve (AUC) of the chromatograms at 280 nm (Figure 14). The straight line of the calibration curve and the R^2 value, the coefficient of determination show that the AUC levels correlate with the concentrations.

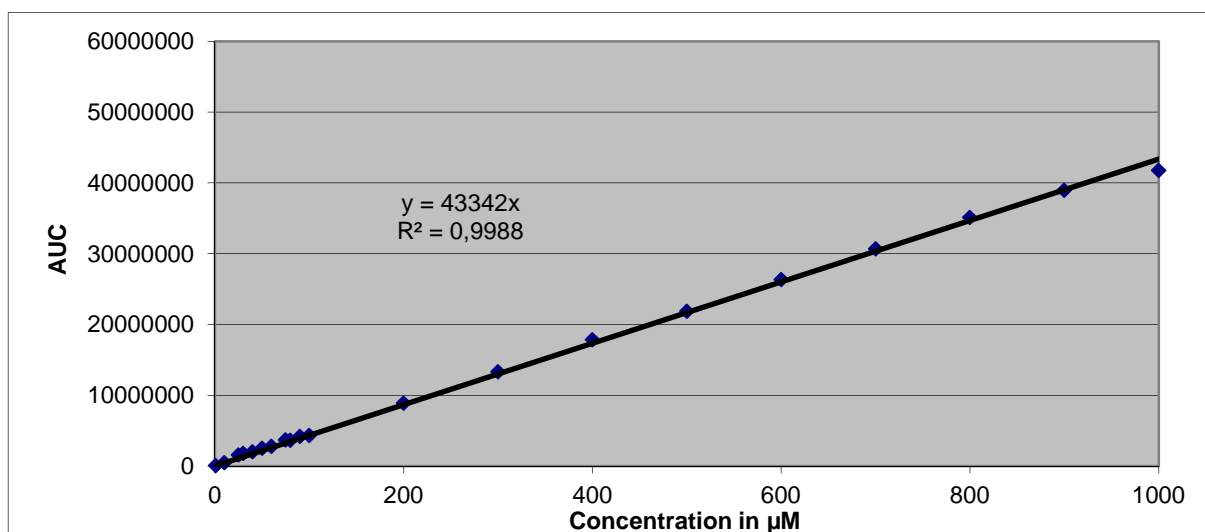


Figure 14 - Calibration curve of CP20

HPLC analysis of CP20 from 2.5 – 1000 μM

6.3 HPO BBB Permeability using non-contact co-culture PBEC model

PBECs were grown in non-contact co-culture, with rat C6 glial cells on the bottom of the transwell (i.e. plated on the 12-well plate underneath the Transwell filter). Transport across the BBB was determined for the HPOs YMF25, YMF24, YMF16 and CP20 as a control. The samples for the HPLC were collected from the basolateral chamber and apical chamber. Moreover samples of the 800 μM HPO solutions were injected in order to determine the amount that was initially added. The assay buffer (HBSS, 25mM HEPES, 0.1% BSA, pH 7.4) was injected in order to correct the AUC.

The HPLC results of the samples from the apical chamber showed that only a small percentage of the initially added amount was left (Table 1). The most important results are those of the basolateral chamber, because they show the amount of the HPO that crossed the BBB. The results obtained from the HPLC were corrected using the sodium fluorescein transfer via the paracellular route. This value was subtracted from the overall transfer, measured by HPLC. For example, in one experiment 15.2 % of CP20 was able to penetrate from the apical chamber into the basolateral chamber. The HPLC results of the other HPOs show the same pattern with only a small percentage left in the apical chamber, between 3-15% in the basolateral chamber and the main part of the compounds inside the cells.

Table 1 HPO Permeability for PBECs in non-contact co-culture

	mean % in apical chamber (blood compartment)	mean % in basolateral chamber (brain compartment)
CP20	0.53	15.17
YMF25	0.14	11.98
YMF24	0.41	14.40
YMF16	0.16	2.92

The results of the basolateral chambers were compared to the *in vivo* data taken from the thesis of Sourav Roy: *Iron chelator design: evaluation of blood-brain barrier permeability and neuroprotective properties* (Roy 2009).

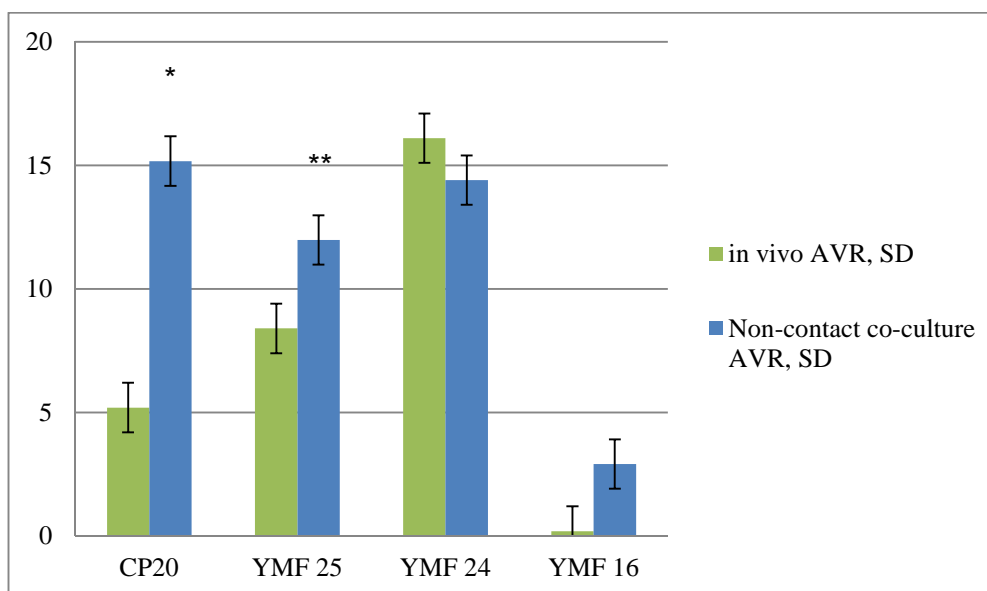


Figure 15 HPO permeability comparison of in vitro (non-contact co-culture) with in vivo data

The graph shows the permeability of the indicated HPO, obtained from in vitro BBB system using PBECs in non-contact co-culture with C6 cells as a BBB model (Blue bars) and in vivo BBB permeability using in situ perfusion of HPO in mice (Green Bars) conducted by Sourav Roy (Roy 2009). * $P < 0.05$, ** $P < 0.01$ when compared to in vivo data.

Both systems showed that CP20, YMF24 and YMF25 are able to cross the BBB. YMF16 achieved the lowest penetration in both systems. Statistical analysis with GradPad Prism using the unpaired t-test showed that the means of YMF24 and YMF16 were not significantly different. However, the means of YMF25 and CP20 were significantly different.

6.4 HPO BBB Permeability using contact co-culture PBEC model

PBECs were grown in contact co-culture, with rat C6 glial cells on the underside of the transwell. Transport across the BBB was determined for the HPOs, YMF25,

YMF24, YMF16 and CP20 as a control. The samples for the HPLC were collected from the basolateral chamber and apical chamber. Moreover samples of the 800 μ M HPO solutions were injected in order to determine the amount that was initially added. The assay buffer (HBSS, 25mM HEPES, 0.1% BSA, pH 7.4) was injected in order to correct the AUC.

The HPLC results of the samples from the apical chamber showed again that only a small percentage of the initially added amount was left. In this model around 8-18% of the HPOs could penetrate into the basolateral chamber (Table 2).

Table 2 HPO Permeability for PBECs in contact co-culture

	mean % in apical chamber (blood compartment)	mean % in basolateral chamber (brain compartment)
CP20	0.07	16.38
YMF25	0.05	6.57
YMF24	0.20	18.28
YMF16	0.05	8.52

The results of the basolateral chambers were compared to the *in vivo* data taken from the thesis of Sourav Roy: *Iron chelator design: evaluation of blood-brain barrier permeability and neuroprotective properties* (Roy 2009).

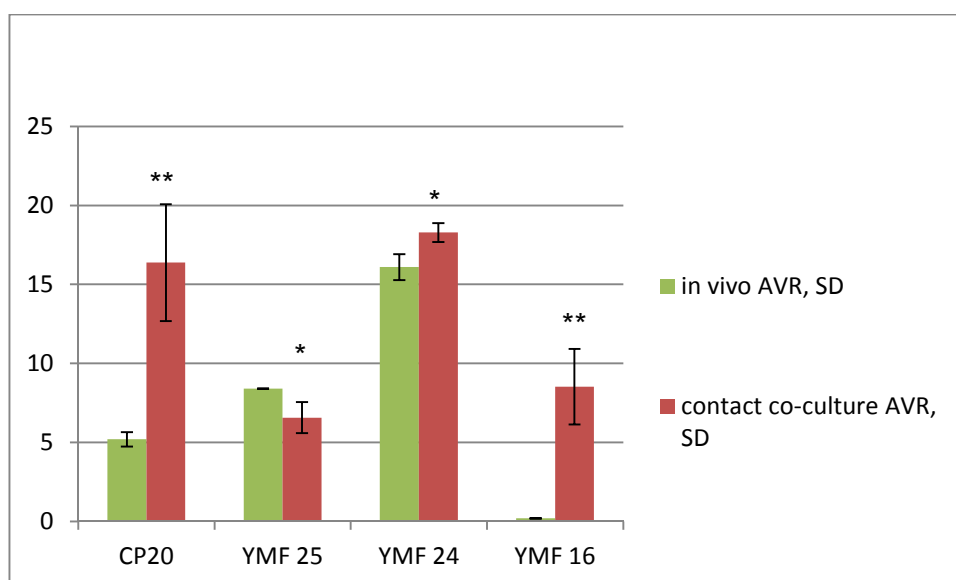


Figure 16 HPO permeability comparison of in vitro (contact co-culture) with in vivo data

The graph shows the permeability of the indicated HPO, obtained from in vitro BBB system using PBECs in contact co-culture with C6 cells as a BBB model (Red bars) and in vivo BBB permeability using in situ perfusion of HPO in mice (Green Bars) conducted by Sourav Roy (Roy 2009). * $P < 0.05$, ** $P < 0.01$ when compared to in vivo data.

In both systems, YMF24 achieved the highest concentration in the basolateral chamber. However, YMF16 achieved a higher concentration than YMF25 and CP20 in the *in vitro* model. Statistical analysis with GradPad Prism using the unpaired t-test showed that all means of the HPOs significantly different.

Furthermore, the results of the contact co-culture were compared with the results of the non-contact co-culture.

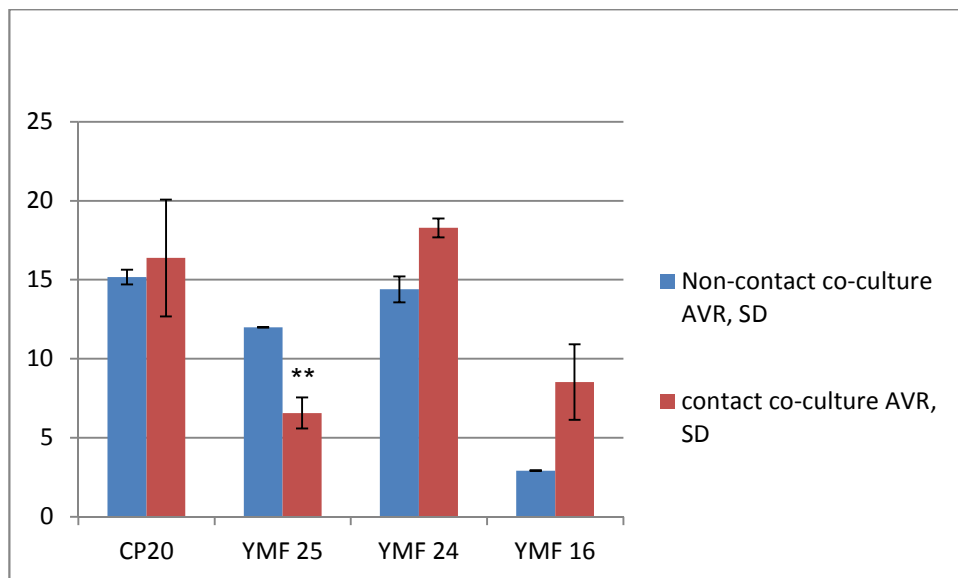


Figure 17 HPO permeability comparison of both in vitro (contact co-culture and non-contact co culture) systems

The graph shows the permeability of the indicated HPO, obtained from both in vitro BBB systems using PBECs in non-contact co-culture with C6 cells as a BBB model (Blue bars) and contact co-culture (Red Bars) * $P < 0.05$, ** $P < 0.01$ when compared to non-contact co-culture data.

Statistical analysis with GradPad Prism using the unpaired t-test showed that the means of YMF24, YMF16 and CP20 were not significantly different, only the means of YMF25 were significantly different.

6.5 HPO BBB Permeability using non-contact co-culture PBEC model

In the last permeability assay PBECs were grown again in non-contact co-culture, because the results of this model were more similar to the *in vivo*-system results. Moreover, this model is simpler than the contact co-culture, thus sources of errors can be reduced. In this permeability assay the assay buffer did not contain protein (BSA), in order to investigate if this would affect the HPLC analysis. Transport across the BBB was determined for the HPOs, YMF25, YMF24, YMF16 and CP20 as a

control. The samples for the HPLC were collected from the basolateral chamber and apical chamber. Moreover samples of the 800 μM HPO solutions were injected in order to determine the amount that was initially added. The assay buffer (HBSS, 25mM HEPES, pH 7.4) was injected in order to correct the AUC.

The HPLC results of the samples from the apical chamber and basolateral chamber are displayed in Table 3. This time a high amount of the HPOs could be detected in the apical chamber, which confirms that even a small percentage of protein in the assay buffer affects the HPLC analysis.

Table 3 HPO Permeability for PBECs in non-contact co-culture

	mean % in apical chamber (blood compartment)	mean % in basolateral chamber (brain compartment)
CP20	72.04	11.03
YMF25	82.06	14.28
YMF24	n/a	20.81
YMF16	80.42	13.83

The results of the basolateral chambers were compared to the *in vivo* data taken from the thesis of Sourav Roy: *Iron chelator design: evaluation of blood-brain barrier permeability and neuroprotective properties* (Roy 2009).

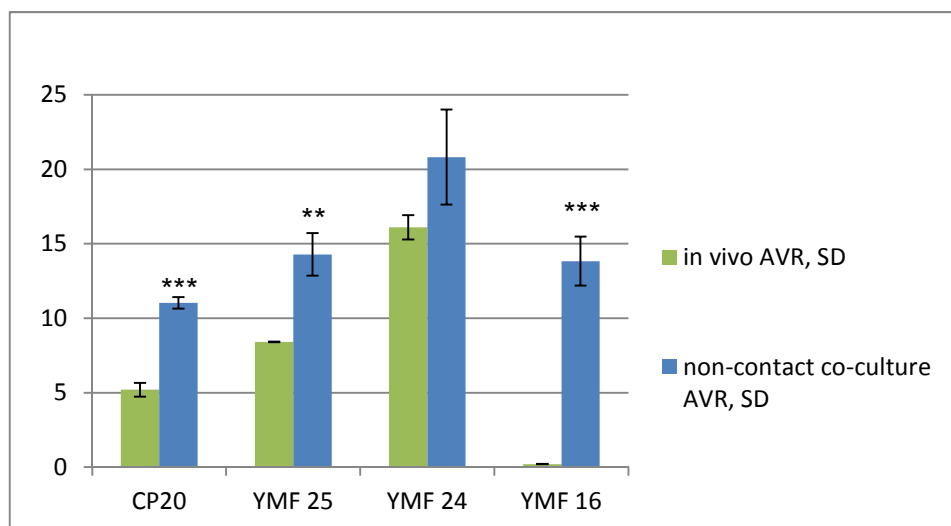


Figure 18 HPO permeability comparison of in vitro (non-contact co-culture) with in vivo data

The graph shows the permeability of the indicated HPO, obtained from in vitro BBB system using PBECs in non-contact co-culture with C6 cells as a BBB model (Blue bars) and in vivo BBB permeability using in situ perfusion of HPO in mice (Green Bars) conducted by Sourav Roy (Roy 2009). ** $P < 0.01$, *** $P < 0.001$ when compared to in vivo data.

Statistical analysis with GradPad Prism using the unpaired t-test showed that the means of YMF24 were not significantly different. However, the means of YMF25, YMF16 and CP20 were significantly different.

Furthermore, the results of the non-contact co-culture were compared with the results of the contact co-culture.

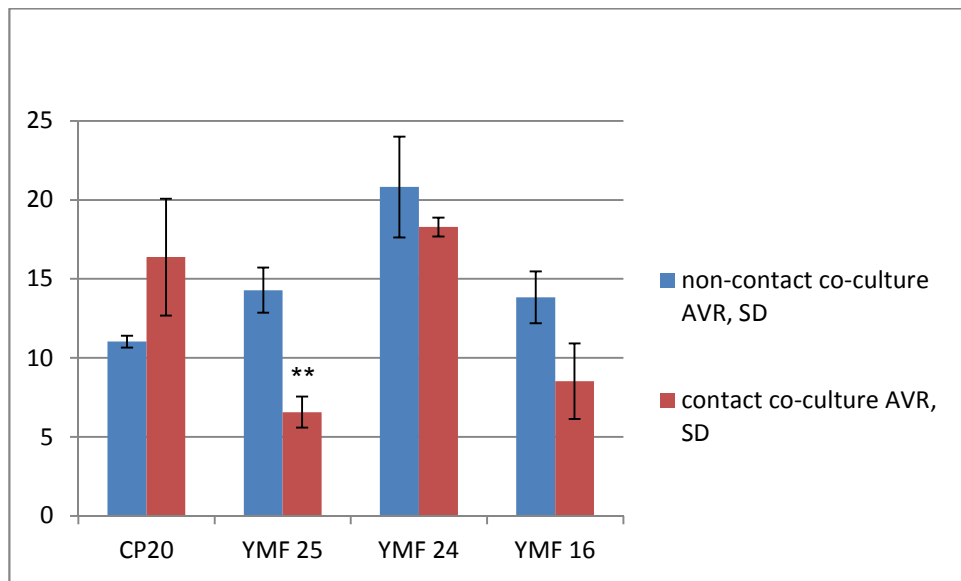


Figure 19 HPO permeability comparison of both in vitro (contact co-culture and non-contact co culture) systems

The graph shows the permeability of the indicated HPO, obtained from both in vitro BBB systems using PBECs in non-contact co-culture with C6 cells as a BBB model (Blue bars) and contact co-culture (Red Bars) * $P < 0.05$, ** $P < 0.01$ when compared to contact co-culture data.

Statistical analysis with GradPad Prism using the unpaired t-test showed that the means of YMF24, YMF16 and CP20 were not significantly different. However, the means of YMF25 were significantly different.

In summary, both *in vitro* systems, non-contact co-culture and contact co-culture, are suitable for the permeability assay of HPOs. The comparison of both *in vitro* models with data obtained from *in vivo* experiments showed similar results. Therefore the non-contact co-culture *in vitro* model should be used for future permeability assays, because it is simpler and thus sources of errors can be reduced.

7 Discussion

The aim of this project was to synthesize an iron chelator, which is coupled with a glucose-molecule and test this chelator for its ability to cross the blood-brain barrier based on an *in vitro* system.

The BBB plays a crucial role in the maintenance of the brain homeostasis and prevents toxic and noxious substrates from entering the brain, including >98% of drugs, while it ensures a sufficient supply of essential nutrients (Mensch, Oyarzabal et al. 2009; Cardoso, Brites et al. 2010). Drug delivery across the BBB is a promising field of research, because the increasing number of neurodegenerative diseases, such as Alzheimer's (AD) and Parkinson's disease (PD), led to the necessity to develop drugs, which can cross the BBB (Molina-Holgado, Gaeta et al. 2008; Mensch, Oyarzabal et al. 2009). There are many experimental systems, which study the function, properties and transport mechanisms of the BBB (Cardoso, Brites et al. 2010).

Iron chelators had been used in diseases with states of iron overload for a long time and are considered as a reasonable approach in the treatment of neurodegenerative diseases, including AD and PD. Both diseases are associated with elevated levels of redox active metals, particularly iron, in the brain, which can lead to toxicity (Hider, Roy et al. 2011). Therefore it is of great interest to investigate the ability of different iron chelators to cross the blood-brain barrier and reach the brain.

Unfortunately the synthesis of the desired iron chelator could not be completed. Due to the limited time available for my project, it was impossible to obtain the desired chelator in acceptable yield and purity. However, a compound was produced with the potential to act as a chelator, made at 12% yield, but needs further work to increase the purity and yield. The conditions of the coupling reaction, such as duration of the coupling and solvents, need to be investigated further. A possibility to obtain a pure product could be purification by column chromatography or extraction. Furthermore, the conditions for the deprotection need to be investigated further. A possible way could be to remove the acetyl groups first. In this order the molecule stays more hydrophobic and it should be extracted more easily into CHCl_3 . Then the cleavage of the benzyl ether could be performed by hydrogenation. A chemist of the

department of Medicinal Chemistry at King's College London will continue to work on this compound with the aim of obtaining the desired iron chelator in an acceptable yield and purity.

Therefore four different HPO-derivatives, CP20, YMF25, YMF24 and YMF16 have been tested on two different *in vitro* systems. The data of the *in vitro* systems was compared to the data obtained from *in vivo* experiments performed by Sourav Roy (Roy 2009). Even though there have been some difficulties with the HPLC analysis, enough valuable data could be produced. The results of my project show, that the non-contact co-culture and the contact co-culture are comparable. Moreover the results of my experiment comply with the results of the *in vivo* experiment, which confirms the quality of the *in vitro* systems. Since YMF24 achieved the highest results in all systems, *in vitro* and *in vivo*, it could be of great interest to continue the research on this molecule. Derivatives of this compound could be synthesized and tested for their ability to cross the BBB.

7.1 Changes in the analysis

As mentioned above, some difficulties appeared with the HPLC analysis. One major problem was the small volume from the apical chamber (~400 μ L) available for analysis. The injector needle of the HPLC did not always reach the bottom of the vial to take up the whole amount needed for the analysis. This made some of the spectra obtained from the apical chamber useless. In order to avoid this problem, the volume can be diluted with water or inserts for the HPLC vials can be used. When the volume is diluted, errors can occur, because the amount has to be corrected afterwards. Moreover, the use of an internal standard would be helpful and ensure that the right amount of the compound was injected. The internal standard should be a HPO-derivative with similar properties to the ones tested, but a difference in the retention time. For this reason CP38 was tested by HPLC analysis, but it is not suitable due to the overlapping retention time.

In order to obtain more accurate data, a calibration curve should be established for each experiment. Moreover it would be interesting to use 100 μ L injections of increasing concentrations of CP20 in assay buffer instead of deionized water.

One limiting factor of the HPLC analysis is the time needed for one sample. By changing the column (PLRP-S, 300 Å, 8 μ m, 15 cm) for a thinner and smaller column

this time could be reduced. Therefore more samples could be analysed in short time and the volume needed would be reduced. Moreover, the faster analysis could prevent the samples from precipitation or other time-depending events.

In addition, some difficulties appeared with the protein assay, which was performed for the non-contact co-culture and contact co-culture. In order to determine the intracellular accumulation of the HPOs, any protein within the sample should be precipitated with TCA. After the centrifuge no pellet was visible. Therefore the samples were analysed by HPLC. The HPLC spectra showed only background signals of the buffer. Our conclusion was that the main part of the HPO was bound to proteins inside the PBECs, which cannot be determined by HPLC. Another method for protein precipitation could be the use of deoxycholate (DOC), acetone, methanol or chloroform instead of TCA. However, one permeability assay using the non-contact co-culture was performed without protein in the assay buffer and the samples analysed by HPLC. In contrast to the results of the other permeability assays, HPLC spectra of the apical chamber showed high amounts of the HPOs (70-80%). In this experiment the results of the apical chamber and the basolateral chamber added up to almost 100%. Consequently, even small amounts of protein in the assay buffer interfere with the HPLC analysis and lead to false results. This needs to be investigated further, in order to determine how much was due to the protein and how much was due to HPLC problems, such as injection errors.

8 Abstract

The blood-brain barrier (BBB) plays a crucial role in maintaining the health and functionality of the central nervous system (CNS). The properties and features of the BBB restrict toxic and noxious substrates, such as xenobiotics, from entering the brain, but provide a sufficient supply of nutrients that are essential for the proper function of the brain. Moreover the BBB prevents > 98% of drugs from entering the brain, hindering side effects within the brain, which is advantageous for most drugs that are not targeted to the brain. However, increased life expectancies have led to an increase in neurodegenerative diseases, such as Alzheimer's (AD) and Parkinson's (PD) and a need to develop drugs that can enter the CNS. AD and PD are associated with elevated levels of redox active metals in the brain, especially iron, which can lead to protein aggregation and produce free radicals, such as hydroxyl radicals. Therefore, chelation therapy is a reasonable approach to reduce the toxic levels of iron, which makes it necessary to design chelating agents that can cross the BBB. Presently, chemists' from Prof Hider's Group at the King's College London (KCL) are working on synthesising different iron chelators using 3-hydroxypyridin-4-one (HPO) derivatives that are linked to a glucose molecule, in order to enhance the BBB permeability of the chelators, since glucose is the main energy source for the brain and therefore is efficiently transported into the brain. The aim of my Diploma thesis project was to synthesize an iron chelator, which is coupled with a sugar molecule and to analyse this molecule's ability to cross the BBB with alongside other HPO-derivative chelators.

The starting material for the chelator synthesis was benzylated maltol, which was converted into the 4-pyridinone-derivative through an amine insertion reaction using β -alanine and sodium hydroxide. For the coupling reaction with the sugar, the 4-pyridinone-derivative was converted into an NHS-ester which led to the desired compound. The molecule was then purified by repeated extraction. To remove the protective groups, benzyl ether and acetic acid ester, the molecule underwent hydrogenation followed by the molecule being taken up in sodium hydroxide, respectively. Unfortunately, this was not successful and could not be repeated due to time restrictions of my project, and so the BBB permeability of the desired compound could not be tested with the other test compounds. The BBB permeability of other

HPO chelators was assessed using in vitro porcine brain endothelial cells (PBECs) co-cultured with glial cells as a BBB model provided by Dr Preston's research group (*Pharmacology and Therapeutics*, KCL). The compounds were tested on PBECs, which were grown with rat C6 glial cell line in non-contact co-culture as well as in contact co-culture. The samples of the permeability assay were analysed and quantified by HPLC.

The results of my experiments showed that both experimental systems are comparable and future permeability assays can be carried out using the non-contact co-culture, which is easier to handle and sources of errors can be reduced. Furthermore, a good correlation between the in vitro data obtained here, and in vivo data (obtained previously by Dr. Sourav Roy using mice models) was observed, which confirms the quality of this experimental system.

9 Zusammenfassung

Die Bluthirnschranke (BHS) spielt eine entscheidende Rolle für die Gesundheit und Funktionalität des zentralen Nervensystems (ZNS). Sie hindert toxische und schädliche Substanzen, wie etwa Xenobiotika ins Gehirn zu kommen, stellt jedoch sicher, dass das Gehirn mit ausreichend essentiellen Nährstoffen versorgt wird. Des Weiteren sorgt die BHS dafür, dass >98% aller Arzneimittel nicht ins Gehirn gelangen, wodurch unerwünschte Nebenwirkungen vermieden werden. Diese Funktion ist für die Mehrzahl der Arzneistoffe erstrebenswert. Mit der Zunahme der Lebenserwartung kam es zu einem Anstieg der neurodegenerativen Erkrankungen, wie Alzheimer und Parkinson, einhergehend mit der Notwendigkeit der Entwicklung von ZNS-gängigen Arzneimitteln. Es besteht ein Zusammenhang zwischen den Erkrankungen, Alzheimer und Parkinson, und erhöhten Werten von redox-aktiven Metallen im Gehirn, insbesondere Eisen, welches zur Aggregation von Proteinen und der Entstehung von freien Radikalen, wie etwa dem Hydroxyl-Radikal führen kann. Chelatbildung ist ein möglicher Ansatz die erhöhten Eisenwerte zu reduzieren und führte zur Entwicklung von Chelatoren, welche die BHS überwinden können. Derzeit arbeiten Chemiker der Arbeitsgruppe von Prof. Hider des King's College London an der Synthese von Eisenchelatoren, die sich von dem 3-Hydroxypyridin-4-on (HPO) ableiten und mit einem Glucosemolekül gekoppelt sind. Durch diese Modifikation soll die Permeabilität durch die BHS erhöht werden, da Glucose die Hauptenergiequelle des Gehirns ist und effizient ins Gehirn transportiert wird. Ziel meiner Diplomarbeit war es einen Eisenchelator zu synthetisieren, der mit einem Zuckermolekül verknüpft ist und diesen, neben anderen HPO-Derivaten, auf seine Eignung die BHS zu überwinden, zu testen.

Ausgangsmaterial für die Synthese des Eisenchelators war benzyliertes Maltol, welches durch Zusetzen von β -Alanin und Natronlauge zum 4-Pyridinon-Derivat umgewandelt wurde. Für die Kopplung mit dem Zucker wurde ein NHS-ester aus dem 4-Pyridinon-Derivat hergestellt, der reaktiver ist und die Kupplungsreaktion verlief erfolgreich. Das Molekül wurde durch wiederholte Extraktion aufgereinigt. Für die Fertigstellung des gewünschten Eisenchelators galt es die Schutzgruppen, Benzylether und Essigsäureester, abzuspalten. Der Benzylether wurde mittels Hydrierung entfernt und das Molekül anschließend mit Natronlauge behandelt, um

die Essigsäureester abzuspalten. Dieser Versuch blieb bedauerlicherweise erfolglos und die Reaktionsbedingungen für die Schutzgruppenabspaltung konnten aufgrund des limitierten Zeitraums leider nicht weiter erforscht werden. Aus diesen Gründen konnte das Molekül nicht mit den anderen HPO-Derivaten auf seine BHS-permeabilität getestet werden. Die BHS-permeabilität der anderen HPO-Chelatoren wurde anhand des *in vitro* Systems bestehend aus Endothelzellen eines Schweinegehirns gemeinsam mit Gliazellen von Ratten in *non-contact co-culture* als auch *contact co-culture* getestet. Beide *in vitro* Systeme wurden von Dr. Prestons Arbeitsgruppe (*Pharmacology and Therapeutics*, KCL) bereitgestellt. Die Proben des Permeabilitätstests wurden mittels HPLC analysiert und quantifiziert.

Die Ergebnisse der Experimente haben ergeben, dass beide *co-culture* Systeme gleichwertig sind und für weitere Permeabilitätstests das *non-contact co-culture* System, welches weniger komplex ist, verwendet werden kann. Des Weiteren konnte eine gute Übereinstimmung zwischen den Ergebnissen der *in vitro* Systeme und *in vivo* Daten (entnommen der Dissertation von Dr. Sourav Roy) beobachtet werden, wodurch die Qualität der *in vitro* Systeme bestätigt wurde.

10 Miscellaneous

10.1 References

- Abbott, N. J. (2002). "Astrocyte-endothelial interactions and blood-brain barrier permeability." Journal of Anatomy **200**(6): 629-638.
- Abbott, N. J., A. A. Patabendige, et al. (2010). "Structure and function of the blood-brain barrier." Neurobiol Dis **37**(1): 13-25.
- Abbott, N. J., L. Ronnback, et al. (2006). "Astrocyte-endothelial interactions at the blood-brain barrier." Nat Rev Neurosci **7**(1): 41-53.
- Aschner, M., V. A. Fitsanakis, et al. (2006). "Blood-brain barrier and cell-cell interactions: methods for establishing in vitro models of the blood-brain barrier and transport measurements." Methods Mol Biol **341**: 1-15.
- Avdeef, A. and O. Tsinman. "Prediction of Caco-2 pH-Dependent Permeability based on High-Quality in vitro Training Set." Retrieved 08.03.2012, from http://www.inforlab-chimie.fr/doc/document_fichier_316.pdf.
- Badgular, N. P. M. e. a. (2006). "N-Carboxymethylated 6,7-Dimethoxy-4-trifluoromethylcarbostyrils as Fluorescence Markers for Amino Acids, Peptides, Amino Carbohydrates and Amino Polysaccharides." Eur. J. Org. Chem.: 2715 - 2722.
- Ballabh, P., A. Braun, et al. (2004). "The blood-brain barrier: an overview: structure, regulation, and clinical implications." Neurobiol Dis **16**(1): 1-13.
- Bergmann, M. and L. Zervas (1964). "Synthesen mit Glucosamin." European Journal of Inorganic Chemistry **64**(5): 978.
- Bernacki, J., A. Dobrowolska, et al. (2008). "Physiology and pharmacological role of the blood-brain barrier." Pharmacol Rep **60**(5): 600-622.
- Burd, L., V. Fraser, et al. (2001). Encyclopedia of Diseases and Disorders.
- Calabria, A. R., C. Weidenfeller, et al. (2006). "Puromycin-purified rat brain microvascular endothelial cell cultures exhibit improved barrier properties in response to glucocorticoid induction." Journal of Neurochemistry **97**(4): 922-933.
- Cappellini, M. D. and P. Pattoneri (2009). "Oral Iron Chelators." Annual Review of Medicine **60**: 25-38.
- Cardoso, F. L., D. Brites, et al. (2010). "Looking at the blood-brain barrier: molecular anatomy and possible investigation approaches." Brain Res Rev **64**(2): 328-363.
- Cecchelli, R., V. Berezowski, et al. (2007). "Modelling of the blood-brain barrier in drug discovery and development." Nat Rev Drug Discov **6**(8): 650-661.
- Cohen-Kashi Malina, K., I. Cooper, et al. (2009). "Closing the gap between the in-vivo and in-vitro blood-brain barrier tightness." Brain Research **1284**: 12-21.
- Dauchy, S., F. Dutheil, et al. (2008). "ABC transporters, cytochromes P450 and their main transcription factors: expression at the human blood-brain barrier." Journal of Neurochemistry **107**(6): 1518-1528.
- Dean, M., A. Rzhetsky, et al. (2001). "The human ATP-binding cassette (ABC) transporter superfamily." Genome Res **11**(7): 1156-1166.
- Dore-Duffy, P. (2008). "Pericytes: pluripotent cells of the blood brain barrier." Curr Pharm Des **14**(16): 1581-1593.
- Ehrlich, P. (1885). Sauerstoff-Bedürfniss des Organismus. Eine farbenanalytische Studie.
- Elkascif, M. N., M. (1960). "The 4-Pyrones. Part I. Reactions of Some 4-Pyrones and 4-Thiopyrones Involving the Ring Oxygen." Journal of the American Chemical Society **82**: 4344-4347.

- EPDA. (2012). "<http://www.parkinsonsawareness.eu.com/en/campaign-literature/prevalence-of-parkinsons-disease/>." Retrieved 21/01/2012.
- Floyd, R. A. and K. Hensley (2002). "Oxidative stress in brain aging. Implications for therapeutics of neurodegenerative diseases." *Neurobiology of Aging* **23**(5): 795-807.
- Forster, C. (2008). "Tight junctions and the modulation of barrier function in disease." *Histochem Cell Biol* **130**(1): 55-70.
- Furuse, M. (2009). "Knockout animals and natural mutations as experimental and diagnostic tool for studying tight junction functions in vivo." *Biochim Biophys Acta* **1788**(4): 813-819.
- Furuse, M., T. Hirase, et al. (1993). "Occludin: a novel integral membrane protein localizing at tight junctions." *J Cell Biol* **123**(6 Pt 2): 1777-1788.
- Gaeta, A. and R. C. Hider (2005). "The crucial role of metal ions in neurodegeneration: the basis for a promising therapeutic strategy." *Br J Pharmacol* **146**(8): 1041-1059.
- Gaeta, A., F. Molina-Holgado, et al. (2011). "Synthesis, physical-chemical characterisation and biological evaluation of novel 2-amido-3-hydroxypyridin-4(1H)-ones: Iron chelators with the potential for treating Alzheimer's disease." *Bioorganic & Medicinal Chemistry* **19**(3): 1285-1297.
- Gkouvatsos, K., G. Papanikolaou, et al. (2011). "Regulation of iron transport and the role of transferrin." *Biochim Biophys Acta*.
- Gumbleton, M. and K. L. Audus (2001). "Progress and limitations in the use of in vitro cell cultures to serve as a permeability screen for the blood-brain barrier." *J Pharm Sci* **90**(11): 1681-1698.
- Hawkins, B. T. and T. P. Davis (2005). "The blood-brain barrier/neurovascular unit in health and disease." *Pharmacol Rev* **57**(2): 173-185.
- Hawkins, R. A., R. L. O'Kane, et al. (2006). "Structure of the blood-brain barrier and its role in the transport of amino acids." *Journal of Nutrition* **136**(1 Suppl): 218S-226S.
- Hermanson, G. (2008). *Bioconjugate Techniques*: 1202.
- Hider, R. C., Y. Ma, et al. (2008). "Iron chelation as a potential therapy for neurodegenerative disease." *Biochem Soc Trans* **36**(Pt 6): 1304-1308.
- Hider, R. C., S. Roy, et al. (2011). "The potential application of iron chelators for the treatment of neurodegenerative diseases." *Metallomics* **3**(3): 239-249.
- Huber, J. D., R. D. Egleton, et al. (2001). "Molecular physiology and pathophysiology of tight junctions in the blood-brain barrier." *Trends Neurosci* **24**(12): 719-725.
- Kim, J. A., N. D. Tran, et al. (2006). "Brain endothelial hemostasis regulation by pericytes." *J Cereb Blood Flow Metab* **26**(2): 209-217.
- Kwiatkowski, J. L. (2008). "Oral iron Chelators." *Pediatric Clinics of North America* **55**(2): 461-+.
- Liu, D. Y., Z. D. Liu, et al. (1999). "Gradient ion-pair high-performance liquid chromatographic method for analysis of 3-hydroxypyridin-4-one iron chelators." *J Chromatogr B Biomed Sci Appl* **730**(1): 135-139.
- Liu, Z. D. and R. C. Hider (2002). "Design of clinically useful iron(III)-selective chelators." *Medicinal Research Reviews* **22**(1): 26-64.
- Lossi, L., S. Alasia, et al. (2009). "Cell death and proliferation in acute slices and organotypic cultures of mammalian CNS." *Prog Neurobiol* **88**(4): 221-245.
- Mensch, J., J. Oyarzabal, et al. (2009). "In vivo, in vitro and in silico methods for small molecule transfer across the BBB." *J Pharm Sci* **98**(12): 4429-4468.
- Molina-Holgado, F., A. Gaeta, et al. (2008). "Neuroprotective actions of deferiprone in cultured cortical neurones and SHSY-5Y cells." *Journal of Neurochemistry* **105**(6): 2466-2476.
- Montalbetti, C. and V. Falque (2005). "Amide bond formation and peptide coupling." *Tetrahedron* **61**: 10827 - 10852.
- Neises, B. and W. Steglich (1978). *Angew. Chem. Int. Ed.* **17**: 522-524.
- Oshiro, S., M. S. Morioka, et al. (2011). "Dysregulation of iron metabolism in Alzheimer's disease, Parkinson's disease, and amyotrophic lateral sclerosis." *Adv Pharmacol Sci* **2011**: 378278.
- Pantopoulos, K. and M. W. Hentze (1995). "Rapid Responses to Oxidative Stress Mediated by Iron Regulatory Protein." *Embo Journal* **14**(12): 2917-2924.

- Papanikolaou, G. and K. Pantopoulos (2005). "Iron metabolism and toxicity." Toxicology and Applied Pharmacology **202**(2): 199-211.
- Pardridge, W. M. (1999). "Blood-brain barrier biology and methodology." J Neurovirol **5**(6): 556-569.
- Parlament, E. (2012). "<http://www.europarl.europa.eu/sides/getDoc.do?pubRef=-//EP//TEXT+TA+P7-TA-2011-0016+0+DOC+XML+V0//EN>." Retrieved 21/01/2012.
- Persidsky, Y., S. H. Ramirez, et al. (2006). "Blood-brain barrier: structural components and function under physiologic and pathologic conditions." J Neuroimmune Pharmacol **1**(3): 223-236.
- Petty, M. A. and E. H. Lo (2002). "Junctional complexes of the blood-brain barrier: permeability changes in neuroinflammation." Prog Neurobiol **68**(5): 311-323.
- Roy, S. (2009). Iron chelator design : evaluation of blood-brain barrier permeability and neuroprotective properties.
- Sanchez-Gonzalez, P. D., F. J. Lopez-Hernandez, et al. (2011). "Effects of deferasirox on renal function and renal epithelial cell death." Toxicology Letters **203**(2): 154-161.
- Sauer, I., I. R. Dunay, et al. (2005). "An apolipoprotein E-derived peptide mediates uptake of sterically stabilized liposomes into brain capillary endothelial cells." Biochemistry **44**(6): 2021-2029.
- Sheftel, A. (2001). "The long history of iron in the Universe and in health and disease." Biochimica Et Biophysica Acta-Biomembranes.
- Smith, M., Y. Omid, et al. (2007). "Primary porcine brain microvascular endothelial cells: biochemical and functional characterisation as a model for drug transport and targeting." J Drug Target **15**(4): 253-268.
- Stevenson, B. R., J. M. Anderson, et al. (1989). "Phosphorylation of the tight-junction protein ZO-1 in two strains of Madin-Darby canine kidney cells which differ in transepithelial resistance." Biochemical Journal **263**(2): 597-599.
- Supplements, O. o. D. (2007). Retrieved 07/01/2012, from <http://ods.od.nih.gov/factsheets/iron>.
- Tosi, G., L. Costantino, et al. (2008). "Polymeric nanoparticles for the drug delivery to the central nervous system." Expert Opin Drug Deliv **5**(2): 155-174.
- Wu, D. F. and A. I. Cederbaum (2003). "Alcohol, oxidative stress, and free radical damage." Alcohol Research & Health **27**(4): 277-284.
- Zlokovic, B. V. (2008). "The blood-brain barrier in health and chronic neurodegenerative disorders." Neuron **57**(2): 178-201.

10.2 Table of Formulas

Formula 1: Deferoxamine	9
Formula 2: Deferiprone.....	9
Formula 3: Deferasirox	9
Formula 4: Structure of the desired iron chelator.....	26
Formula 5: Structures of the tested HPO-derivatives	28

10.3 Table of Figures

Figure 1: Schematic representation of chelate ring formation in metal-ligand complexes (taken from Liu and Hider (2002)).....	14
Figure 2: Schematic representation of the NUV (taken from Mensch, Oyarzabal et al. (2009)).....	16
Figure 3: Structure of the BBB tight junctions (taken from Abbott, Patabendige et al. (2010). Further explanation in the text.....	18
Figure 4: Pathways across the BBB (taken from Abbott, Ronnback et al. (2006). Further explanation in the text.	20
Figure 5: Schematic drawings of three in vitro BBB culture systems (taken from Cohen-Kashi Malina, Cooper et al. (2009)).....	24
Figure 6: Schematic representation of the transendothelial electrical resistance measurement with electrodes (taken from Cardoso, Brites et al. (2010)).....	25
Figure 7: 12mm Transwell with 0.4µm pore polycarbonate membrane insert (taken from sigmaaldrich.com)	29
Figure 8: 96 well plate (taken from phenixresearch.com)	31
Figure 9: CP20 HPLC	53
Figure 10: CP20 from Post-Doc Yongmin Ma.....	54
Figure 11: YMF25 800µM in assay buffer, RT ~ 11 minutes	54
Figure 12: YMF24 800µM in assay buffer, RT ~ 12 minutes	55
Figure 13: YMF16 800µM in assay buffer, RT ~ 10 minutes	55
Figure 14: Calibration curve of CP20.....	56
Figure 15: HPO permeability comparison of in vitro (non-contact co-culture) with in vivo data	57
Figure 16: HPO permeability comparison of in vitro (contact co-culture) with in vivo data	58
Figure 17: HPO permeability comparison of both in vitro (contact co-culture and non-contact co culture) systems	59
Figure 18: HPO permeability comparison of in vitro (non-contact co-culture) with in vivo data	60
Figure 19: HPO permeability comparison of both in vitro (contact co-culture and non-contact co culture) systems	61

10.4 Table of Schemes

Scheme 1: Synthesis of 2-methyl-3-benzyloxy-pyran-4(1H)-one	33
Scheme 2: Synthesis of 1-(2'-carboxyethyl)-2-methyl-3-(benzyloxy)-4(1H)-pyridinone	34
Scheme 3: Synthesis of 1-[2'-[(succinimidyl)oxy]carbonyl]ethyl-2-methyl-3-benzyloxy)-4(1H)-pyridinone.....	35
Scheme 4: Synthesis of 1,3,4,6-tetra-O-acetyl- β -D-glucosamine hydrochloride	36
Scheme 5: Synthesis of N-(1,3,4,6-tetra-O-acetyl-2-deoxy- β -D-glucopyranos-2-yl)-3-(3-(benzyloxy)-2-methyl-4-oxopyridin-1(4H)-yl)propanamide	38
Scheme 6: Deprotection of N-(1,3,4,6-tetra-O-acetyl-2-deoxy- β -D-glucopyranos-2-yl)-3-(3-(benzyloxy)-2-methyl-4-oxopyridin-1(4H)-yl)propanamide	39

10.5 Table of Tables

Table 1: HPO Permeability for PBECs in non-contact co-culture57
Table 2: HPO Permeability for PBECs in contact co-culture.....58
Table 3: HPO Permeability for PBECs in non-contact co-culture60

10.6 List of Abbreviations

$^1\text{H-NMR}$ – ^1H -nuclear magnetic resonance
ABC-transporters – ATP-binding cassette transporter
ACN – acetonitrile
AD – Alzheimer's disease
AJ – adherens junctions
AMT – absorptive-mediated transcytosis
AUC – area under the curve
BBB – blood-brain barrier
BCEC – brain capillary endothelial cells
BSA – bovine serum albumin
 CHCl_3 – chloroform
CNS – central nervous system
CP20 – deferiprone
 D_2O – deuterated water
DCC – dicyclohexylcarbodiimide
DCM – dichloromethane
DCU – dicyclohexylurea
DMEM – Dulbecco's Modified Eagle's Medium – low glucose
DMF – dimethylformamide
DMSO – dimethyl sulfoxide
DOC – deoxycholate
EC – endothelial cell
ESI – electrospray ionization
EtOAc – ethyl acetate
EtOH – ethanol
GLUT-1 – glucose transporter-1
HAMP – hepcidin gene
HBSS – Hank's Buffered Salt Solution
HCl – hydrochloric acid
HEPES – 4-(2-hydroxyethyl)-1-piperazineethanesulfonic acid
HH – hereditary hemochromatosis
HPLC – high pressure liquid chromatography
HPO – 3-hydroxypyridin-4-one

JAM – junctional adhesion molecules
JH – juvenile hemochromatosis
KCL – King’s College London
m/z – mass-to-charge ratio
MeOD – deuterated methanol
MHz - megahertz
MP – melting point
MS – mass spectrometry
n/a – not applicable
Na₂SO₄ – sodium sulfate
NaCl – sodium chloride
NaF – sodium fluorescein
NaOH – sodium hydroxide
ND – neurodegenerative diseases
NHS-ester – *N*-Hydroxysuccinimide ester
NVU – neurovascular unit
PBEC – porcine brain endothelial cell
PBS – phosphate-buffered saline
PD – Parkinson’s disease
ppm – parts per million
R² – coefficient of determination
RMT – receptor mediated transcytosis
ROS – reactive oxygen species
RT – retention time
SN – substantia nigra
TCA – Trichloroacetic acid
TEER – transendothelial electric resistance
Tf – transferrin
TJ – tight junctions
TLC – thin layer chromatography

10.7 Curriculum vitae

Personal details

Name	Anna Preisner
Date of birth	July, 30 th 1987
Nationality	Austria
Address	Rennbahnweg 46/1/37 1220 Vienna

Academic Studies

Since October 2005	Pharmacy studies at the University of Vienna
Oct 2011 – Feb 2012	Erasmus student at King's College London Diploma thesis project

Education

Sept 1993 – Jun 1997	Elementary School: VS der Schulbrüder 1210 Vienna
Sept 1997 – Jun 2005	Secondary school: BG Theodor-Kramer Schule, 1220 Vienna

Work experience

Oct 2007 – Sept 2011	office <i>Polcommerce</i>
----------------------	---------------------------

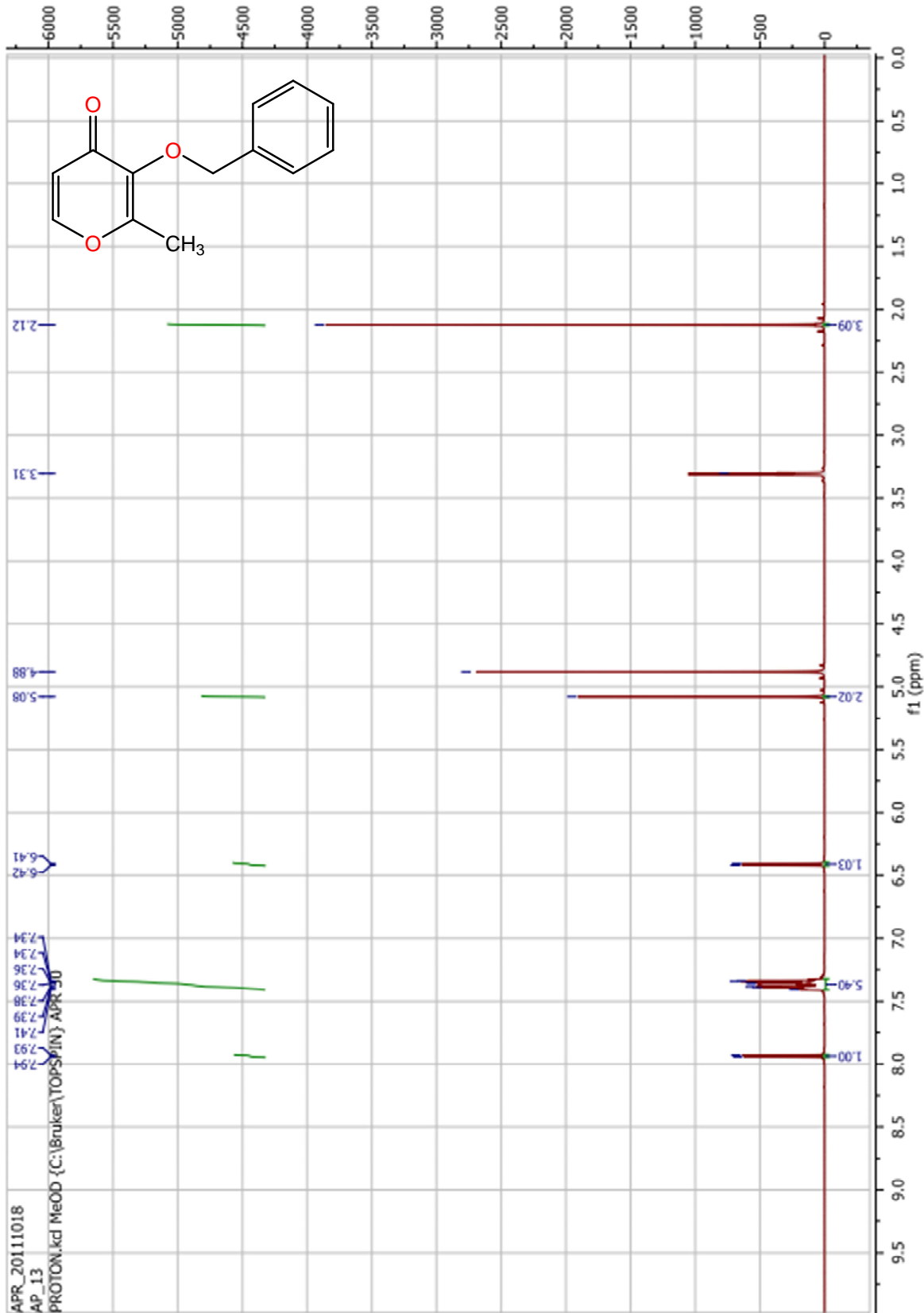
Language skills:

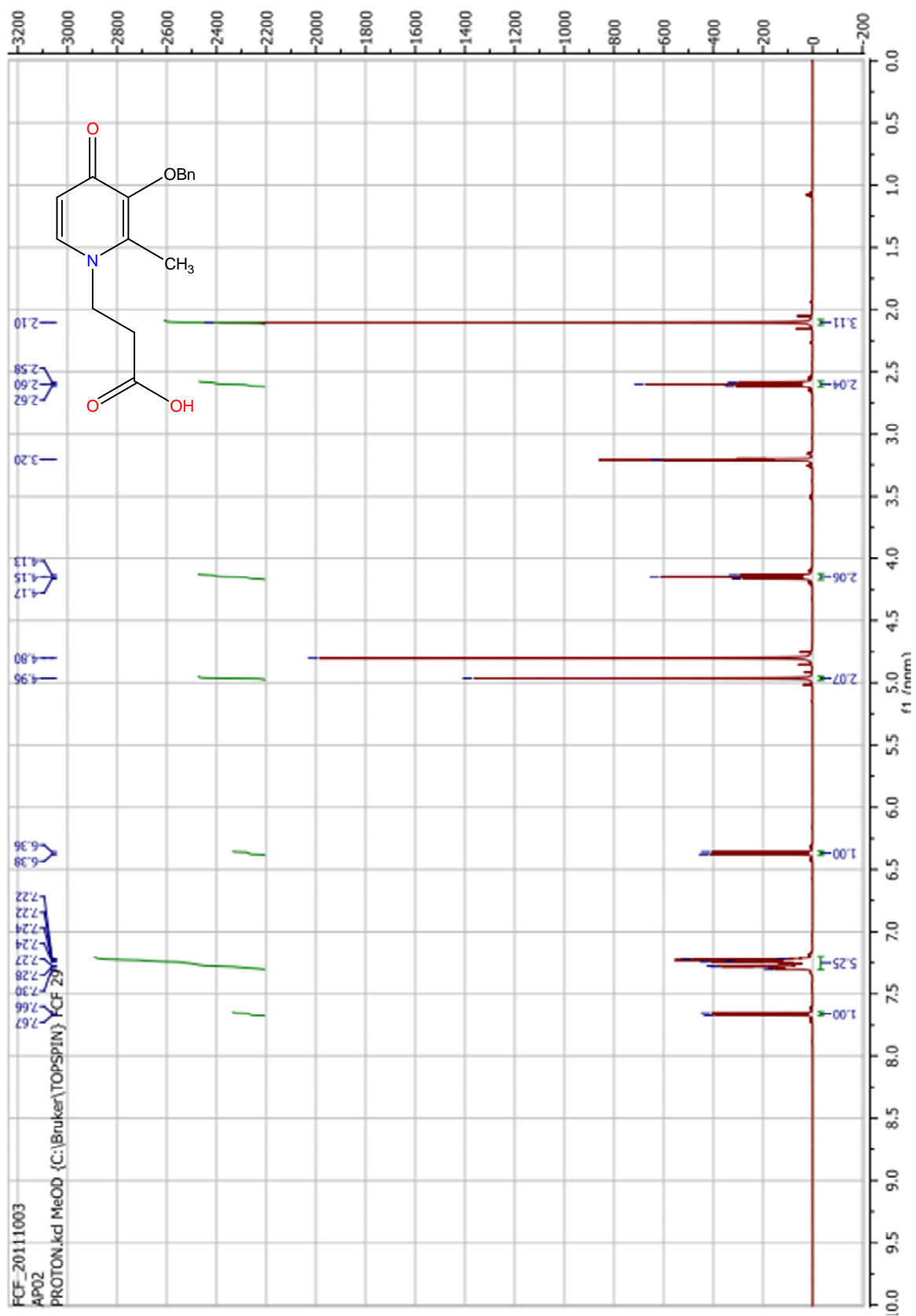
English, fluent in speech and writing
Polish, fluent in speech

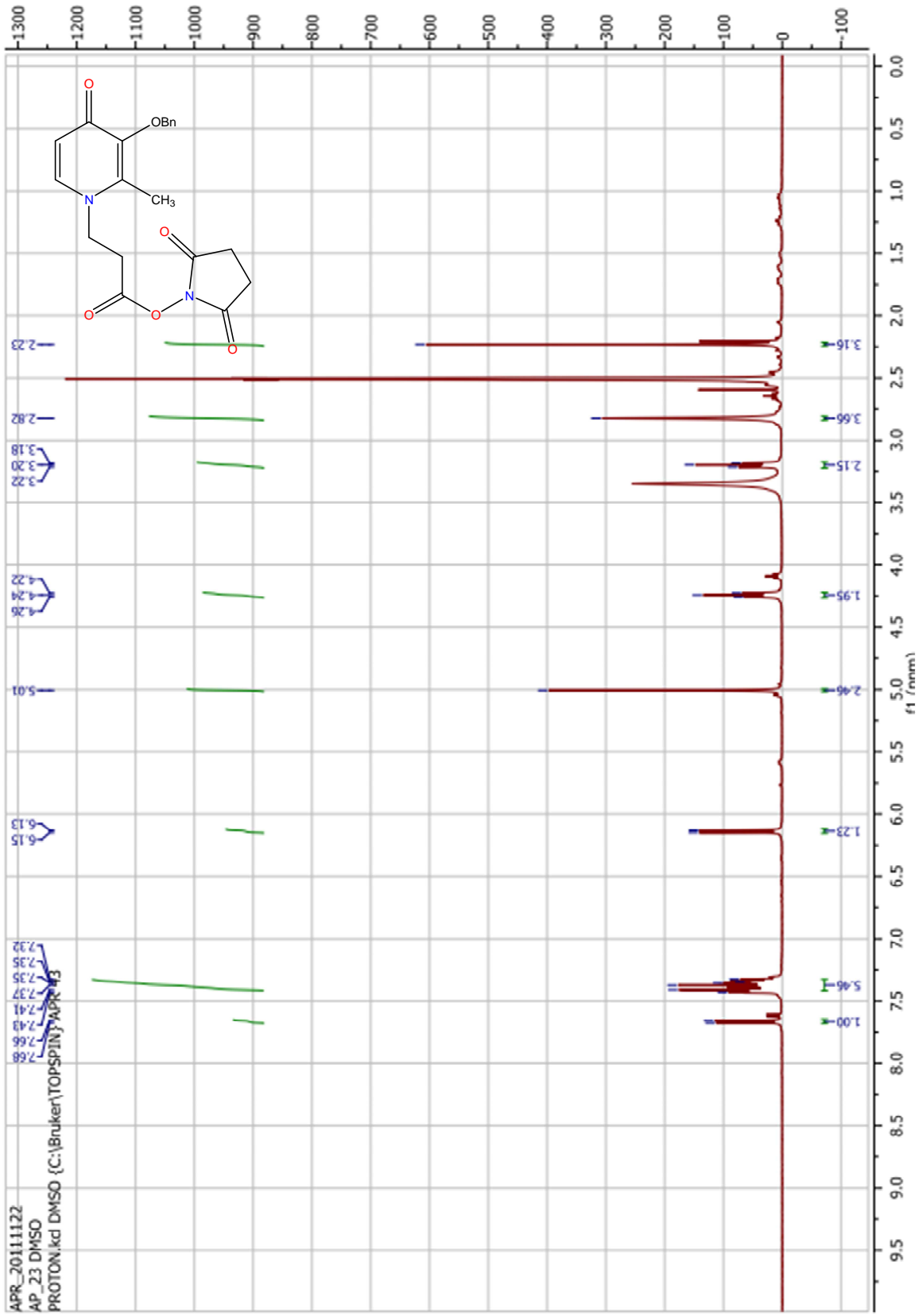
Appendix

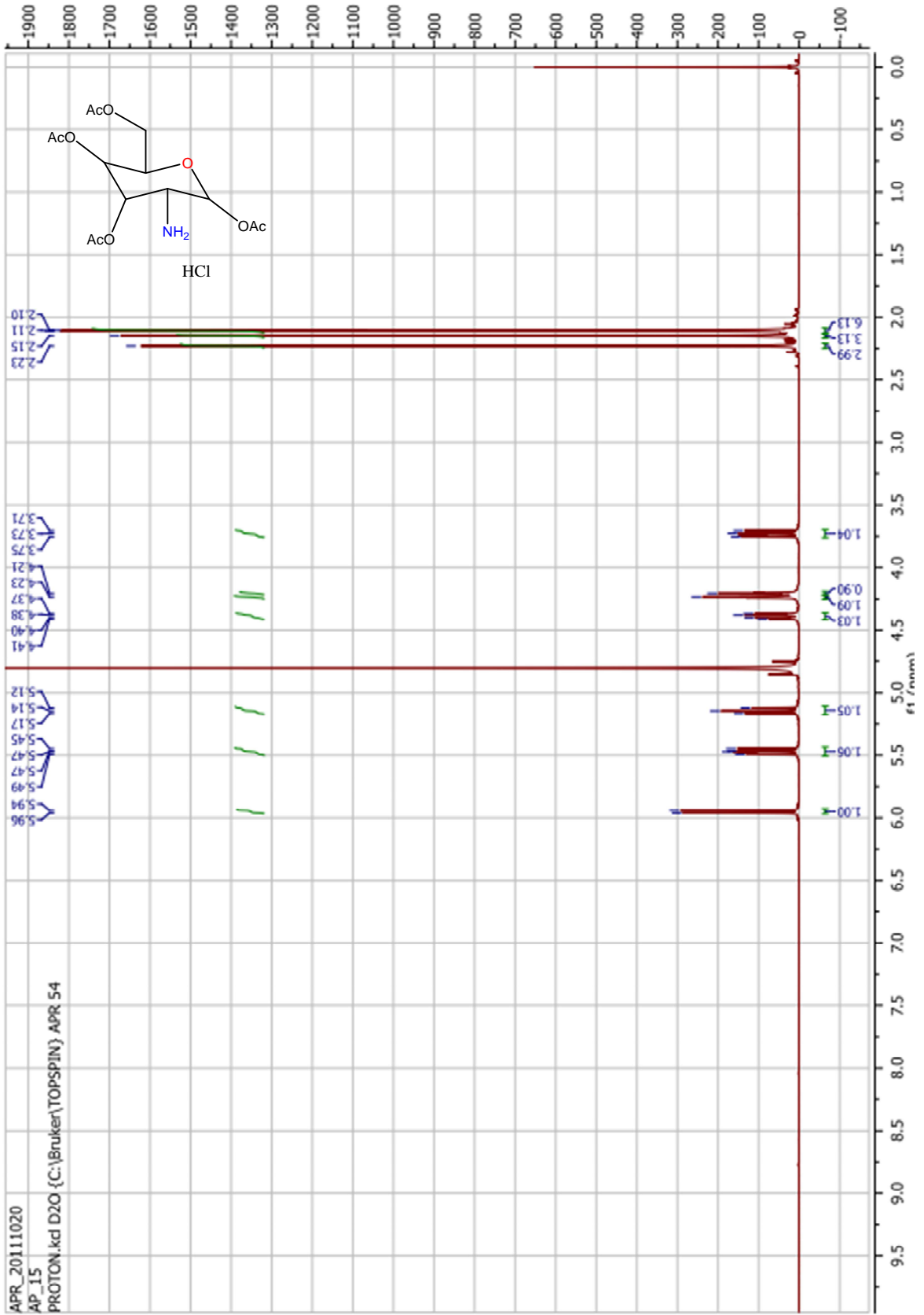
<u>NMR-selected data</u>	II
<u>Mass spectrometry - spectrum</u>	VII
<u>HPLC – AUCs of CP20 in water</u>	VIII
<u>Picture of the research group</u>	X
<u>To Whom It May Concern – by Professor R.C. Hider</u>	XI

NMR-selected data







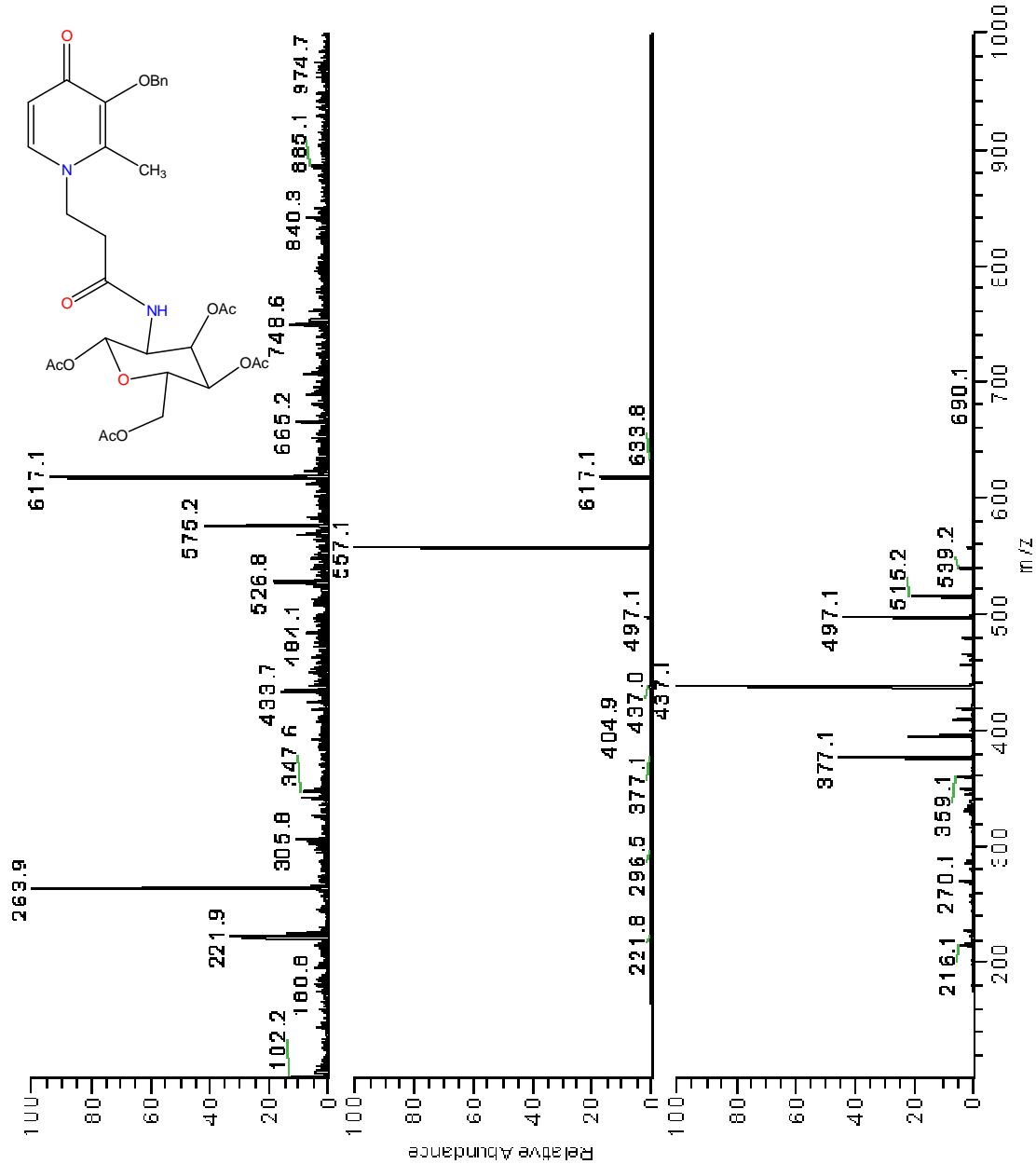


Mass spectrometry - spectrum

NL: 1.65F8
 M17171#192-198 RT:
 8.26-8.35 AV: 7 F: + p ESI
 Full ms [100.00-1000.00]

NL: 1.41E8
 M17171#120-144 RT:
 1.86-2.31 AV: 25 F: + p
 ESI Full ms2
 617.00@cid25.00
 [165.00-1000.00]

NL: 4.57E7
 M17171#170-183 RT:
 2.84-3.10 AV: 14 F: + p
 ESI Full ms3
 617.00@cid25.00
 557.00@cid35.00
 [175.00-1000.00]



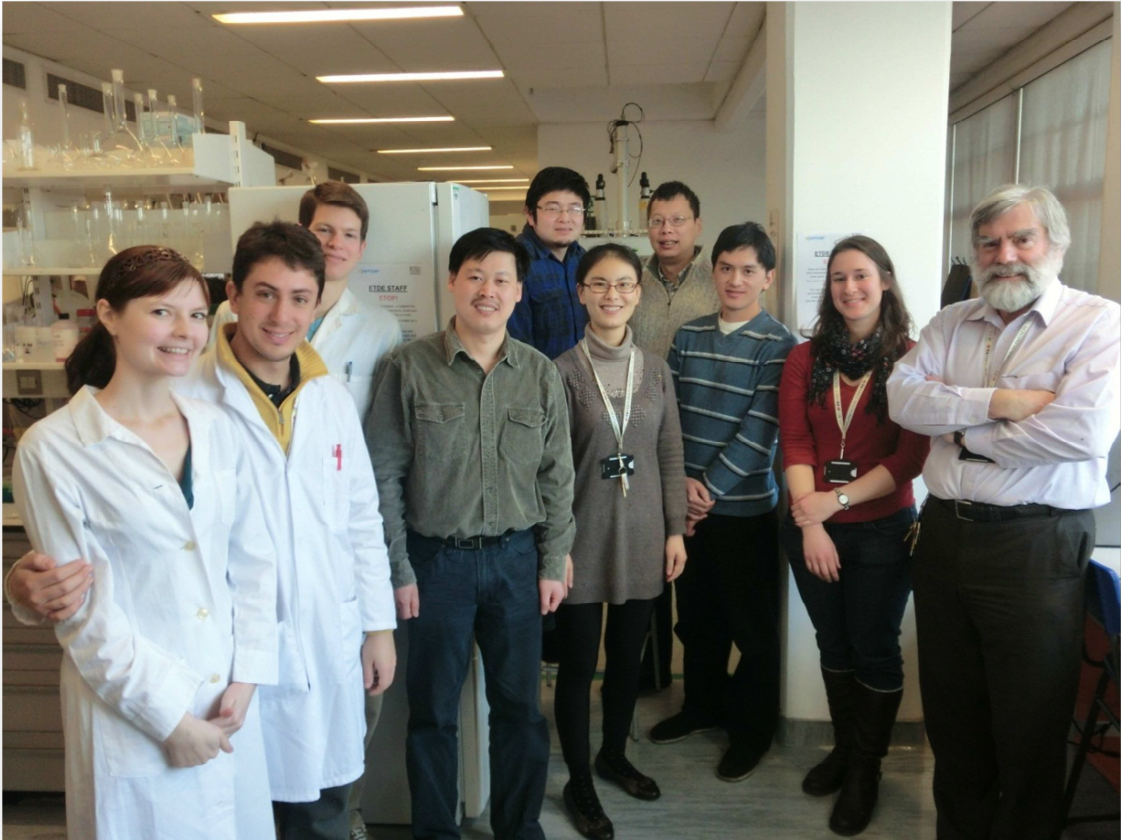
M17171 – AP 29, MW 616 or 347, 5 ul/1 ml 0.1 % FA in MeOH:H2O, 1:1, ESI, MS & MSMS

HPLC – AUCs of CP20 in water

calibration curve CP20 in deionized water		
concentration	AUC	average
2.5µM	360313	
	526581	511643
	648035	
5µM	537162	
	545566	588239
	681989	
10µM	475939	
	494713	485995
	487333	
25µM	1488219	
	1483851	1550140,67
	1678352	
30µM	1705984	
	1781548	1795344,67
	1898502	
40µM	2139638	
	2038625	2072735
	2039942	
50µM	3162483	
	2850783	2889947
	2656575	
60µM	2802289	
	2876229	2859150,67
	2898934	
75µM	3980570	
	3697499	3847354,33
	3863994	
80µM	3638168	
	3662614	3681819,33
	3744676	
90µM	4104965	
	4189063	4200296,33
	4306861	
100µM	4295713	
	4339984	4364541,33
	4457927	
200µM	8752846	

	8894893	8876452,67
	8981619	
300µM	13649953	
	13209635	13390817
	13312863	
400µM	17361178	
	17521684	17519930
	17676928	
500µM	21735932	
	21746765	21842142
	22043729	
600µM	26218820	
	26326481	26323560,3
	26425380	
700µM	30506597	
	30451513	30575400,3
	30768091	
800µM	35204559	
	35197514	35291496,7
	35472417	
900µM	38814056	
	37974499	38561231
	38895138	
1000µM	41120066	
	41833336	41716983
	42197547	

Picture of the research group



Picture of Professor Hider's research group at King's College London.

To Whom It May Concern – by Professor R.C. Hider

**School of Biomedical
& Health Sciences**
Pharmaceutical
Science Division

Professor R C Hider
Emeritus Professor
of Medicinal Chemistry

Franklin-Wilkins Building
100 Stamford Street
London SE1 9NH
Tel +44 (0)20 7840 4882
robert.hider@kcl.ac.uk

KING'S
College
LONDON

8.2.12

To whom it may concern

Anne Preisner

Anne Preisner worked with the Medicinal Chemistry Group at King's College London, under the supervision of Professor R. C. Hider for the period October 2011 until mid February 2012. She joined a project centred on the identification of lead molecules for the treatment of Parkinson's disease. As well as making an important contribution to the synthetic efforts of the laboratory, she worked closely with Dr Jane Preston of the Blood Brain Barrier Group, also based at King's College. During her studies with Dr Preston she obtained the first useful correlation between a cell culture system and animal perfusion studies. This has important implications for the Parkinson's disease project. Anna proved to be an extremely careful and meticulous worker in the laboratory and we placed much weight on her results. Her project should be rated very highly by the University of Vienna.



R C Hider

Professor of Medicinal Chemistry

www.kcl.ac.uk